Supporting Information

Mollebenzylanols A and B, Highly Modified and Functionalized Diterpenoids with a 9-Benzyl-8,10-dioxatricyclo[5.2.1.0^{1,5}]decane Core from *Rhododendron molle*

Junfei Zhou, Junjun Liu, Ting Dang, Haofeng Zhou, Hanqi Zhang, and Guangmin Yao*

Hubei Key Laboratory of Natural Medicinal Chemistry and Resource Evaluation, School of Pharmacy, Tongji Medical College, Huazhong University of Science and Technology, Wuhan 430030, China.

List of Contents

* To whom correspondence should be addressed. E-mail: gyap@mail.hust.edu.cn

Table S1. ^{1}H (400 MHz) and ^{13}C NMR (100 MHz) Spectroscopic Data for Compounds 1, 2, and 1a.

no.	**1**[a]		**2**[a]		**1a**[b]	
	δ_H (J in Hz)	δ_C	δ_H (J in Hz)	δ_C	δ_H (J in Hz)	δ_C
1	2.00, dd (7.5, 3.6)	53.0	2.50, t (8.5)	48.6	2.74, dd (4.4, 3.9)	54.2
2	3.72, dd (7.5, 6.6)	84.3	3.86, dd (8.5, 7.3)	76.6	5.53, dd (4.4, 3.0)	88.0
3	3.50, d (6.6)	89.1	3.55, d (7.3)	89.4	5.80, d (3.0)	88.7
4		41.4		40.6		43.5
5		99.2		98.2		100.5
6	3.93, dd (10.1, 1.7)	82.0	3.87, dd (9.8, 1.4)	81.3	4.37, dd (10.3, 1.7)	80.2
7a	2.96, d (14.2, 1.7)	39.0	3.02, dd (14.2, 1.4)	40.2	3.14, dd (14.2, 1.7)	38.7
7b	2.82, d (14.2, 10.1)		2.65, dd (14.2, 9.8)		3.04, dd (14.2, 10.3)	
8		140.7		140.8		140.3
9	7.07, br s	130.9	7.06, br s	130.9	7.33, br s	130.8
10		139.1		139.1		138.6
11	7.01, br d (7.6)	128.1	7.00, br d (7.6)	128.1	7.08, br d (7.0)	127.9
12	7.15, t (7.6)	129.4	7.14, t (7.6)	129.4	7.30, t (7.0)	129.2
13	7.04, br d, (7.6)	127.3	7.02, br d (7.6)	127.3	7.33, br d (7.0)	127.3
14		111.1		111.1		110.5
15	2.10, qd (7.0, 3.6)	52.2	2.41, dq (8.5, 7.3)	46.7	2.67, qd (6.9, 3.9)	54.0
16	1.36, s	17.4	1.34, s	16.4	1.54, s	17.9
17	2.31, s	21.6	2.31, s	21.6	2.25, s	21.8
18	1.07, s	19.3	1.05, s	19.6	1.38, s	18.3
19	1.20, s	26.3	1.22, s	26.4	1.49, s	25.7
20	1.24, d (7.0)	14.5	1.03, d (7.3)	13.7	1.44, d (6.9)	14.5
1′						166.0
2′						129.0
3′					8.13, d (8.5)	132.2
4′					7.69, d (8.5)	132.7
5′						129.8
6′					7.69, d (8.5)	132.7
7′					8.13, d (8.5)	132.2
1″						165.9
2″						129.0
3″					8.10, d (8.5)	132.3
4″					7.65, d (8.5)	132.8
5″						129.9
6″					7.65, d (8.5)	132.8
7″					8.10, d (8.5)	132.3

[a]Recorded in methanol-d_4. [b]Recorded in pyridine-d_5.

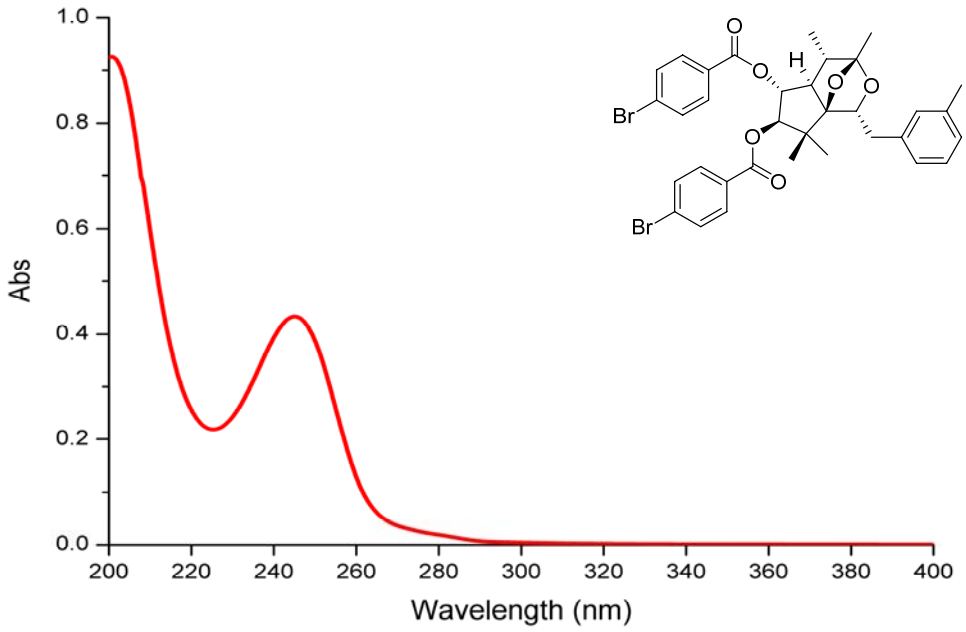

Figure S1. UV spectrum of **1a** in methanol.

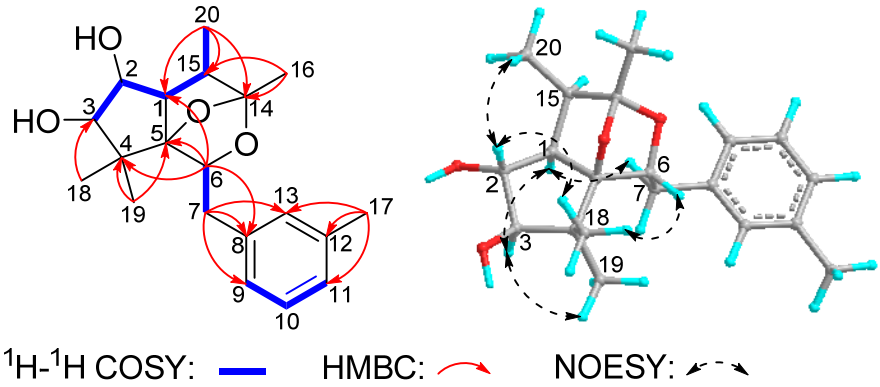

Figure S2. ^{1}H–^{1}H COSY, HMBC, and NOESY correlations of **2**.

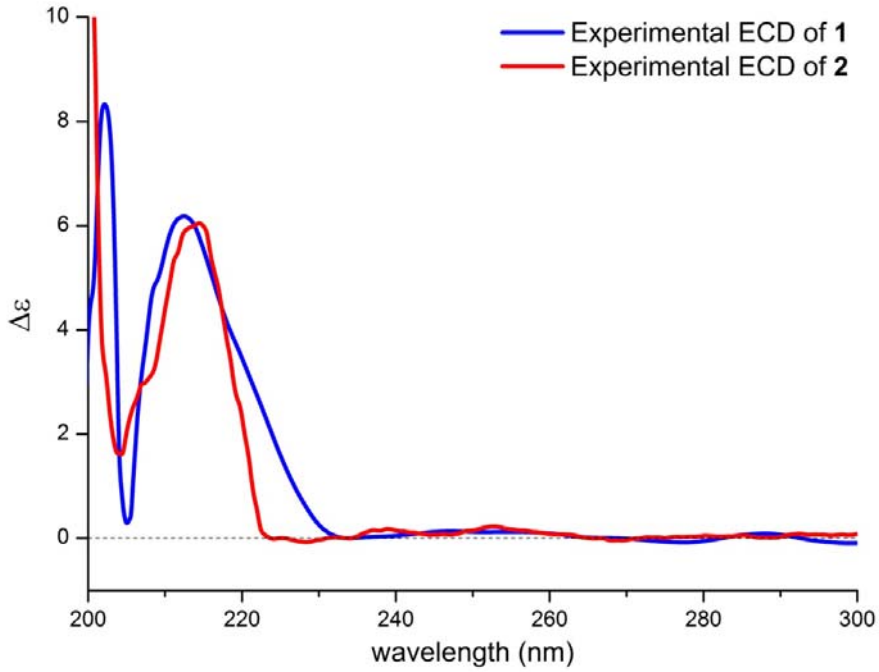

Figure S3. The experimental ECD spectra of **1** and **2** in methanol.

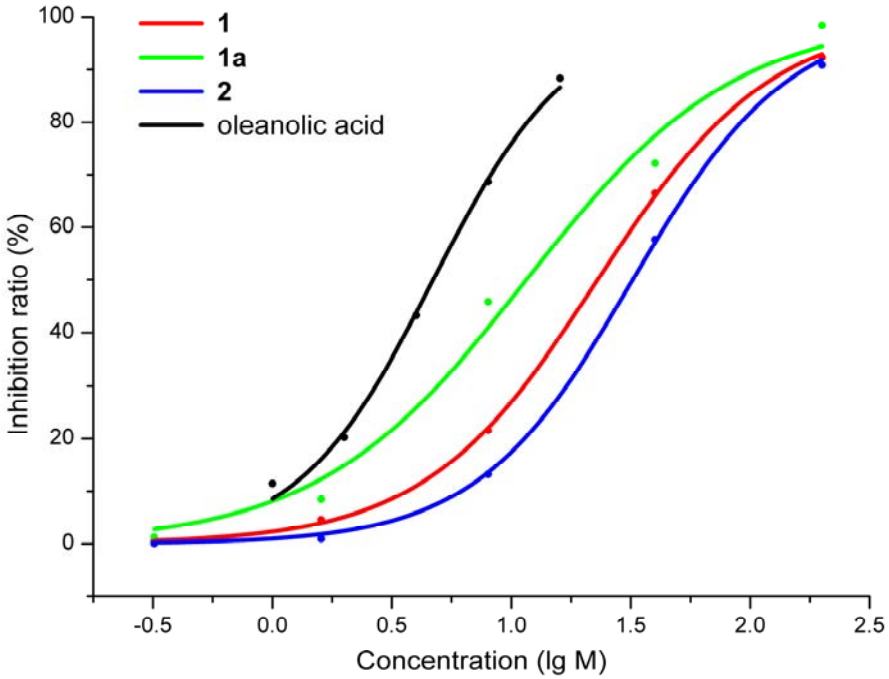

Figure S4. Concentration−inhibition ratio curves of mollebenzylanols A (**1**) and B (**2**), **1a**, and oleanolic acid.

The final concentration of oleanolic acid was 1, 2, 4, 8, and 16 μM. The final concentration of mollebenzylanols A (**1**) and B (**2**) as well as **1a** were 0.32, 1.6, 8, 40, and 200 μM.

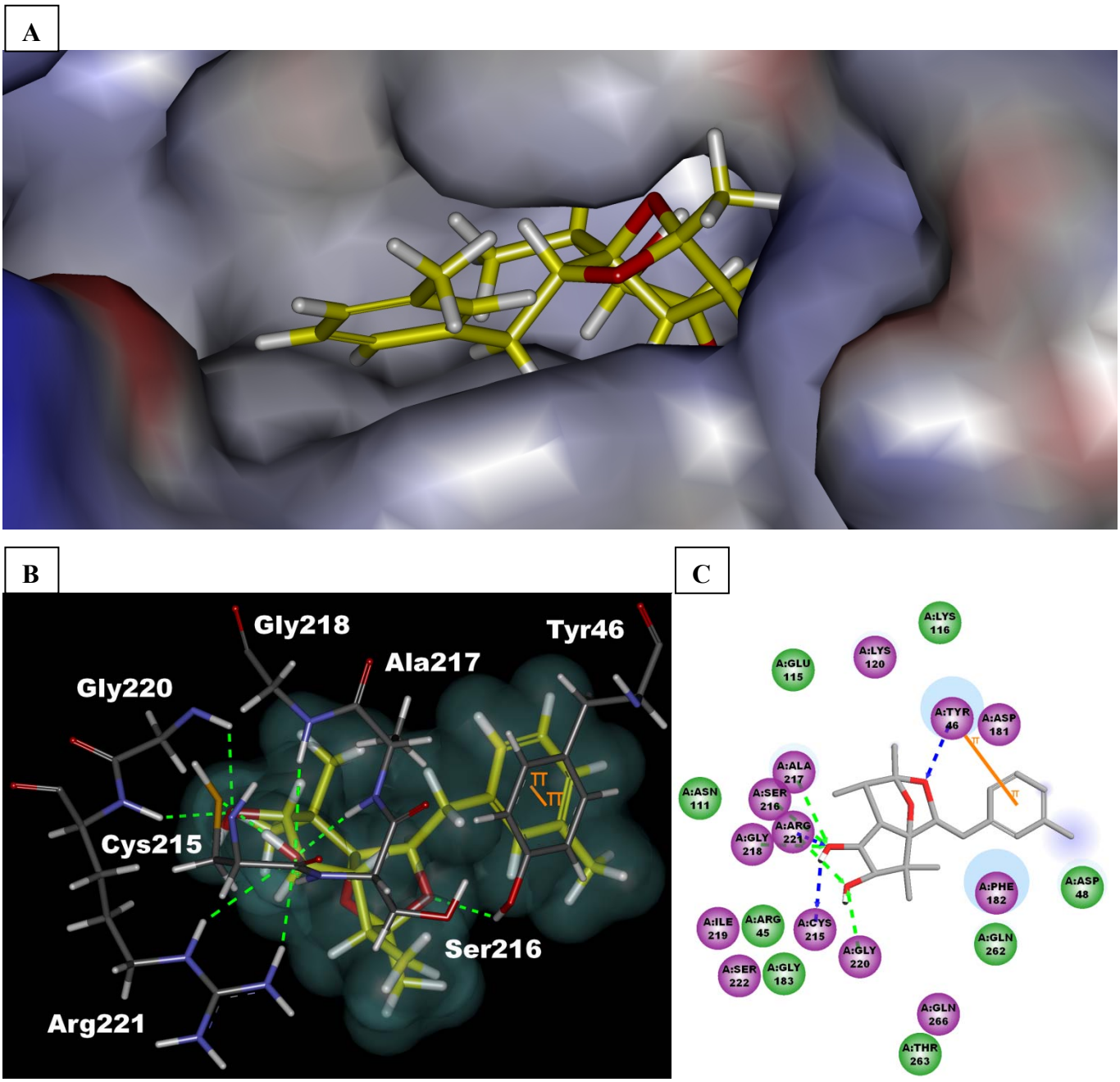

Figure S5. Molecular docking models for PTP1B inhibition of mollebenzylanol A (**1**).

A: 3D docking surface of the PTP1B protein active site and mollebenzylanol A (**1**).

B and **C**: ligand interaction models of mollebenzylanol A (**1**).

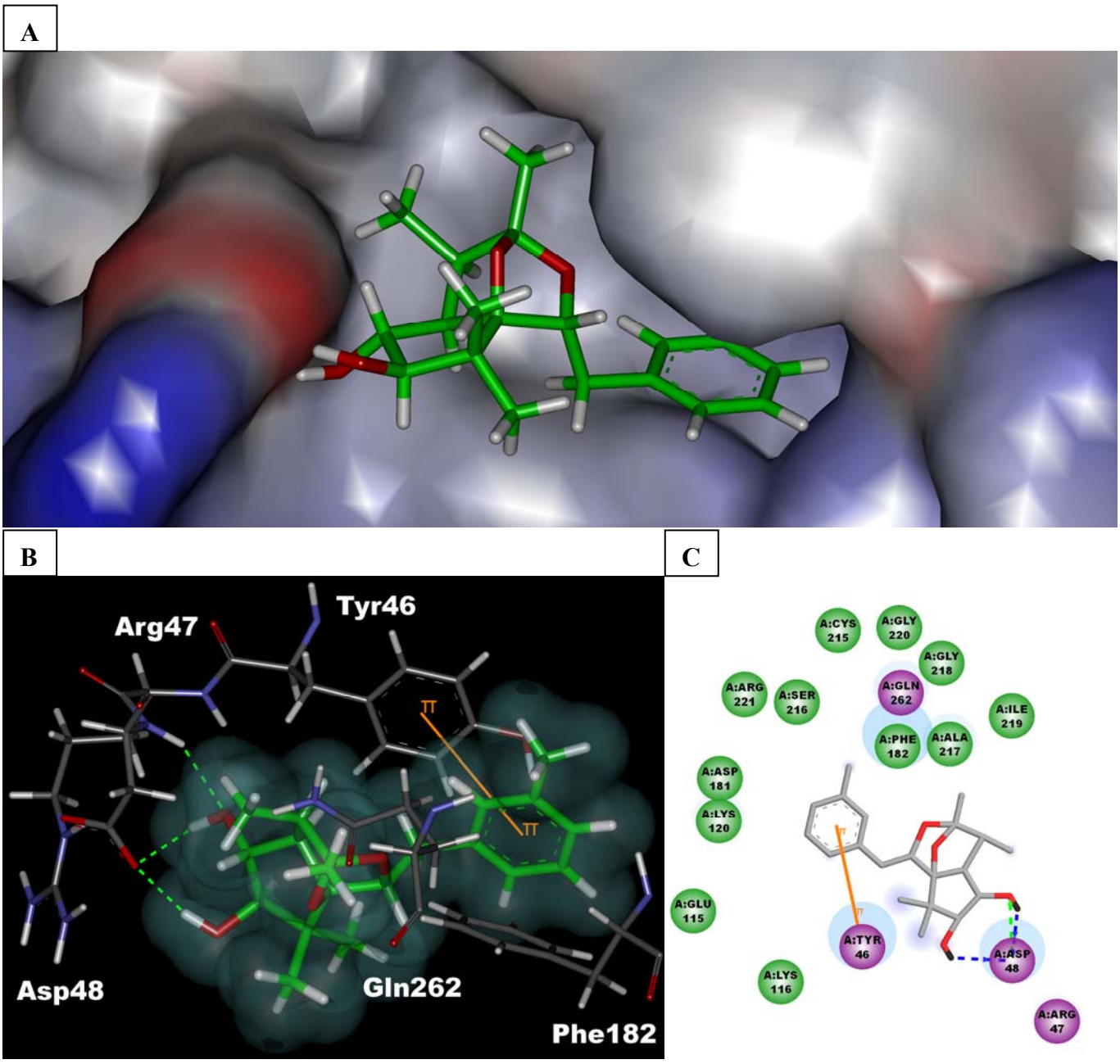

Figure S6. Molecular docking models for PTP1B inhibition of mollebenzylanol B (**2**).

A: 3D docking surface of the PTP1B protein active site and mollebenzylanol B (**2**).

B and **C**: ligand interaction models of mollebenzylanol B (**2**).

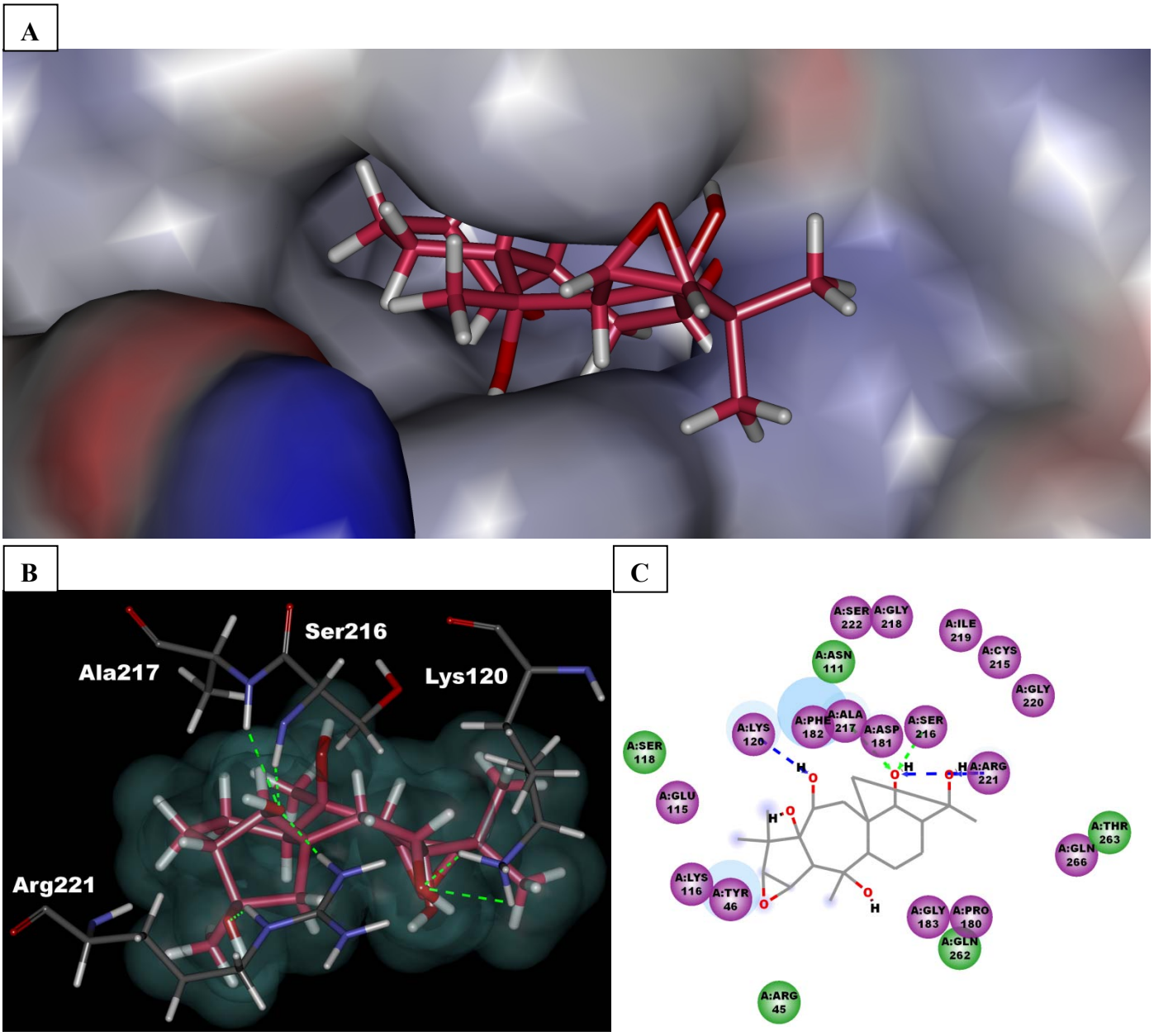

Figure S7. Molecular docking models for PTP1B inhibition of rhodojaponin III (**3**).

A: 3D docking surface of the PTP1B protein active site and rhodojaponin III (**3**).

B and **C**: ligand interaction models of rhodojaponin III (**3**).

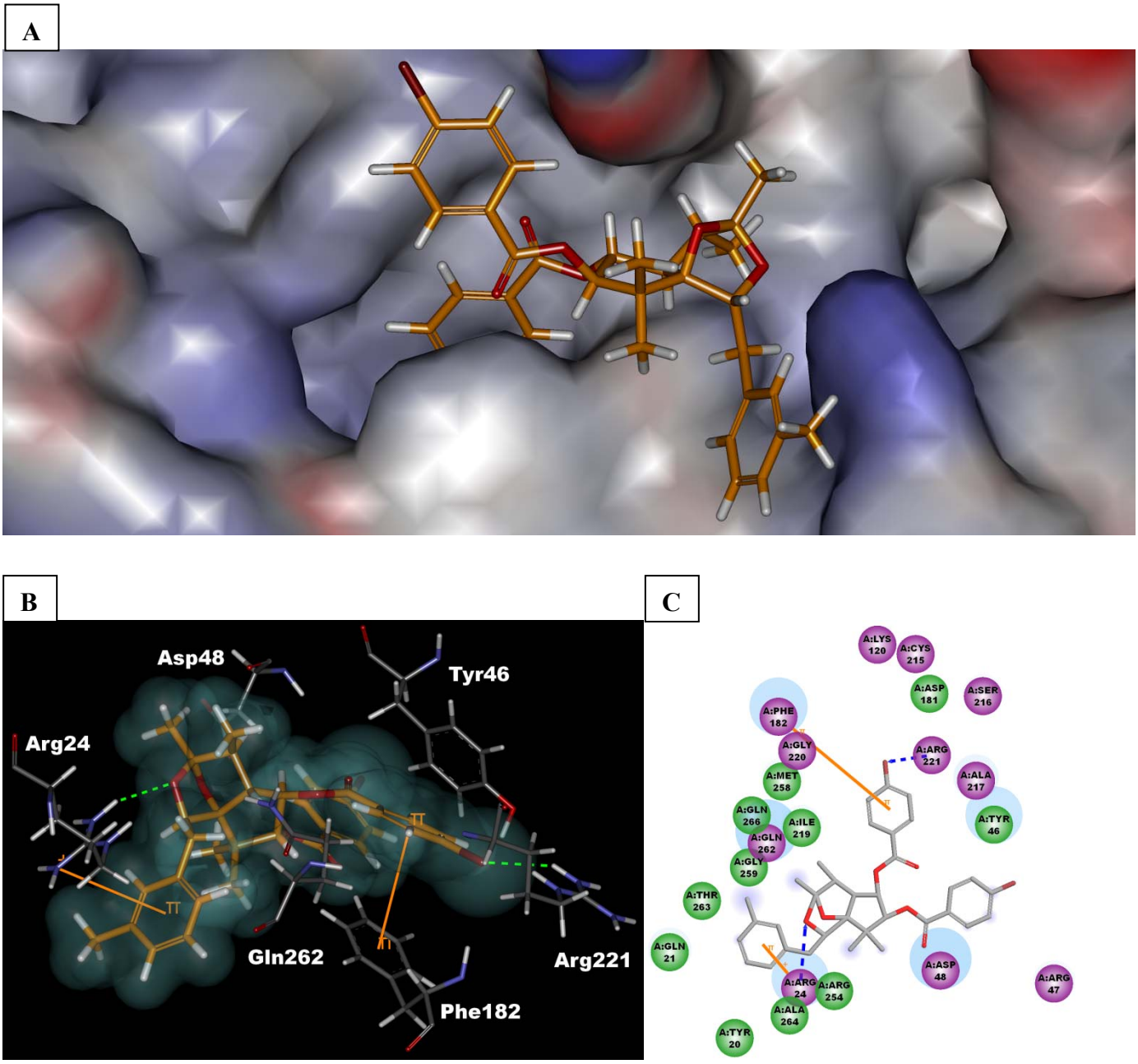

Figure S8. Molecular docking models for PTP1B inhibition of **1a**.

A: 3D docking surface of the PTP1B protein active site and **1a**.

B and **C**: ligand interaction models of **1a**.

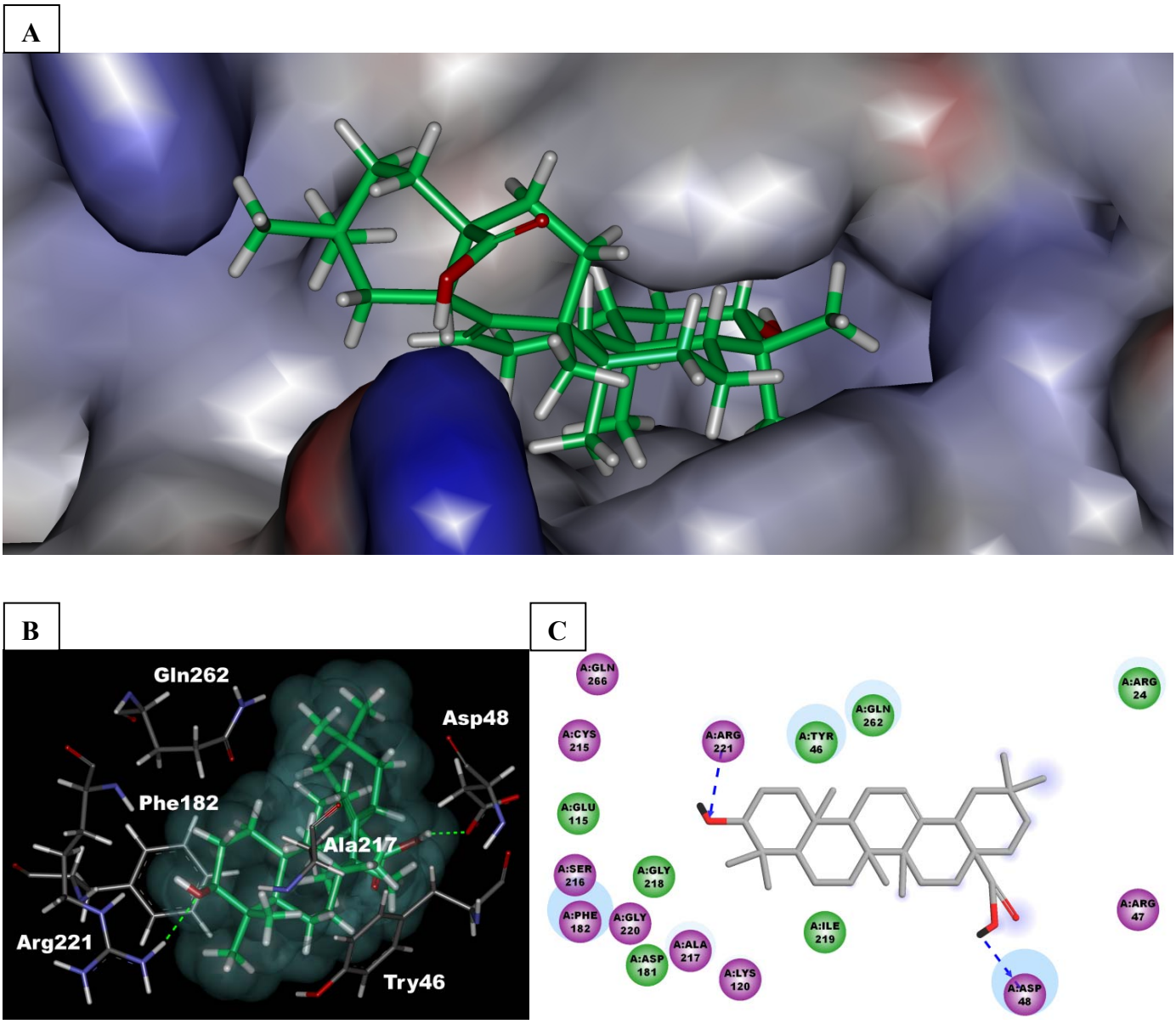

Figure S9. Molecular docking models for PTP1B inhibition of oleanolic acid.

A: 3D docking surface of the PTP1B protein active site and oleanolic acid.

B and **C**: ligand interaction models of oleanolic acid.

Table S2. The Energies (kcal/mol) analysis of 1−3, 1a, and oleanolic acid to PTP1B by Autodock 4.2.6.

Compound	**1**	**2**	**3**	**1a**	oleanolic acid
Binding Energy	−6.15	−6.00	−4.76	−7.94	−8.20
Intermolecular Energy	−7.34	−7.19	−6.25	−10.32	−9.09
Internal Energy	−2.25	−1.03	−2.39	−1.54	0.13
Torsional Energy	1.19	1.19	1.49	2.39	0.89
Unbound Extended Energy	−2.25	−1.03	−2.39	−1.54	0.13
K_i	31.09 μM	91.38 μM	322.63 μM	1.52 μM	978.89 μM

Experimental Section

General Experimental Procedures.

A Beijing Tech X-5 microscopic melting point apparatus was applied for recording on the melting points of single crystals. Optical rotations of compounds **1**−**3** and **1a** were measured using a Perkin-Elmer 341 polarimeter in MeOH. The NMR spectra were determined on a Bruker AM-400, and the ^{1}H (400 MHz) and ^{13}C (100 MHz) NMR chemical shifts were referenced to the solvent residual peaks for methanol-d_4 at δ_H 3.31 and δ_C 49.15 and pyridine-d_5 at δ_H (7.22, 7.58, 8.74) and δ_C (123.87, 135.91, 150.35), respectively. HRESIMS data were acquired on a Bruker micrOTOF II spectrometer for compounds **1**−**3** and **1a** in a positive ion mode. The crystallographic data were obtained on a Bruker SMART APEX-II CCD diffractometer equipped with graphite-monochromatized Cu Kα radiation (λ = 1.54178 Å) for compound **1a**. Samples were purified by semi-preparative HPLC using an Agilent 1200 or Dionex P680 quaternary system with a UV detector and a semi-preparative column (5 μm, 10 × 250 mm, Welch Ultimate XB-C_{18} or XB-phenyl) in a flow rate of 1.5 mL/min. Silica gel (Qingdao Marine Chemical Factory in China), ODS with 50 μm (ODS-A-HG, YMC Co. Ltd., Japan), Sephadex LH-20 (GE Healthcare Bio-Sciences AB, Sweden), and MCI gel (Mitsubishi Chemical Corp., Tokyo, Japan) were applied for column chromatography.

Plant Material.

The leaves of *Rhododendron molle* G. Don were collected at the Qichun, Hubei province, P. R. China, in May 2014. The material was identified by Prof. Jianping Wang, Hubei Key Laboratory of Natural Medicinal Chemistry and Resource Evaluation, School of Pharmacy, Tongji Medical College, Huazhong University of Science and Technology. A voucher specimen (No. 20140520) has been deposited in the department.

Extraction and Isolation.

Dried leaves (25 kg) of *R. molle* were powered and extracted with EtOH−H_2O (95:5, v/v) (5 × 120 L) at room temperature (7 days each). Concentration of the combined percolates under reduced pressure afforded

a dark brown crude extract (3.7 kg). The corresponding extract (3.7 kg) was suspended in distilled water and partitioned with petroleum ether (PE), $CHCl_3$, EtOAc, and *n*-BuOH (seven times each), yielding PE (335.0 g), $CHCl_3$ (1190.0 g), EtOAc (160.0 g), and *n*-BuOH (1155.0 g) fractions. The PE fraction (335.5 g) was separated by a silica gel column (100−200 mesh) with an eluent of PE−acetone (15:1−0:1, v/v) to get six fractions (A−F) on the basis of TLC analysis. Fraction C (eluted with PE−acetone 5:1, 31.8 g) was further resolved on a silica gel column (200−300 mesh) and eluted in a gradient of PE−acetone (8:1−0:1, v/v) to obtain six fractions (C1−C6). Fraction C1 (eluted by PE−acetone 8:1, 4.9 g) was chromatographed on a Sephadex LH-20 column eluted with MeOH to yield five subfractions C1A−C1E. Subfraction C1A (1.2 g) was loaded onto an ODS C_{18} column and eluted in a gradient of MeOH−H_2O (1:9−10:0, v/v) to afford six parts (C1Aa−C1Df). Subfraction C1Ad (eluted by 40% MeOH, 90.3 mg) was further purified by RP C_{18} HPLC, with MeCN−H_2O (70:30, v/v) 1.5 mL/min to obtain compounds **1** (t_R 41.6 min, 8.3 mg, 0.0000332 %) and **2** (t_R 45.3 min, 2.6 mg, 0.0000104 %).

The $CHCl_3$ fraction (1190 g) was separated by a silica gel column (100−200 mesh) with an eluent of CH_2Cl_2−Acetone (20:1−0:1, v/v) to get six fractions (A−F) on the basis of TLC analysis. Fraction D (eluted with CH_2Cl_2−Acetone 3:1, 102.5 g) was further resolved on a silica gel column (200−300 mesh) and eluted in a gradient of PE−Acetone (8:1−0:1, v/v) to obtain six fractions (D1−D6). Fraction D3 (eluted by PE−Acetone 3:1, 8.9 g) was chromatographed on a Sephadex LH-20 column eluted with methanol to yield four subfractions D3A−D3D. Subfraction D3A (1.9 g) was loaded onto an ODS C_{18} column and eluted in a gradient of MeOH−H_2O (1:9−10:0, v/v) to afford four parts (D3Aa−D3Dd). Subfraction D3Aa (eluted by 10% MeOH, 720 mg) was subjected to chromatography on a silica gel column (300−400 mesh) using PE−Acetone (5:1 to 0:1) to yield four subfractions D1Aa1−D1Aa4. Finally, subfraction D1Aa2 (eluted by PE−Acetone 3:1, 110.3 mg) was further purified by RP C_{18} HPLC, with MeOH−H_2O (60:40, v/v) 1.5 mL/min, to yield compound **3** (t_R 29.2 min, 12.9 mg, 0.0000516 %).

*Mollebenzylanol A (**1**):*

A white amorphous powder; $[\alpha]^{20}_{D}$ + 26.5 (*c* 0.1, MeOH); UV (MeOH) λ (log ε): 260.2 (2.29) nm; ECD (MeOH): λ ($\Delta\varepsilon$) 212.4 (+ 6.18) nm; IR (KBr) ν_{max} 3358, 2959, 2890, 1636, 1454, 1372, 1346, 1189, 1117, 1068, 962, 928, 851 cm^{-1}; HR-ESI-MS $[M + Na]^+$ *m/z* 333.2049 (calcd for $C_{20}H_{29}O_4$, 333.2066). ^1H and ^{13}C NMR data, Table S1.

*Mollebenzylanol B (**2**):*

A white amorphous powder; $[\alpha]^{20}_{D}$ + 19.2 (*c* 0.1, MeOH); UV (MeOH) λ (log ε): 262.0 (2.22) nm; ECD (MeOH) λ ($\Delta\varepsilon$) 214.4 (+ 6.05) nm; IR (KBr) ν_{max} 3436, 2962, 2890, 1636, 1458, 1374, 1189, 1067, 1040, 959, 926 cm^{-1}; HR-ESI-MS $[M + Na]^+$ *m/z* 333.2052 (calcd for $C_{20}H_{29}O_4$, 333.2066). ^1H and ^{13}C NMR data, Table S1.

Preparation of 2,3-*O*-(4-Bromobenzoyl)-mollebenzylanol A (1a).

Compound **1** (5.0 mg) and *p*-bromobenzoyl chloride (65.0 mg) were added into 1 mL of anhydrous pyridine, respectively. The mixture was stirred for 4 hours at room temperature. After completion of the reaction, the majority of solvent was separated by reversed-phase semi-preparative HPLC using MeCN in water (90:10) as the mobile phase to give **1a** (7.4 mg, 70.6 %).

*2,3-O-Di-(4-Bromobenzoyl)-mollolide A (**1a**):*

Colorless prisms; mp 193−194 °C; $[\alpha]^{20}_{D}$ − 16.8 (*c* 0.1, MeOH); UV (MeOH) λ_{max} (log ε) 200.6 (3.96), 245.0 (3.64); ECD (MeOH) λ ($\Delta\varepsilon$) 208.4 (+ 17.32), 233.6 (+ 17.01), 252.0 (− 37.21) nm; IR (KBr) ν_{max} 3345, 2960, 2885, 1721, 1590, 1450, 1396, 1368, 1274, 1183, 1109, 1069, 961, 927, 849, 757 cm^{-1}; HR-ESI-MS $[M + Na]^+$ *m/z* 719.0602 (calcd for $C_{34}H_{34}Br_2NaO_6$, 719.0620). ^1H and ^{13}C NMR data, Table S1.

Single-crystal X-Ray Diffraction Analysis and Crystallographic Data for 1a.

Crystal X-ray diffraction data was measured on a Bruker APEX-II CCD diffractometer through a graphite-monochromatized Cu Kα radiation (λ = 1.54178 Å) at 173(2) K. Data was collected by Bruker APEX2 software. Bruker SAINT was applied to data reduction. Structure solution and refinement were performed with the SHELXTL program package. All non-hydrogen atoms were refined anisotropically. The

hydrogen atom positions were geometrically idealized and allowed to ride on their parent atoms.

*Crystallographic Data for **1a**:*

Empirical formula: $C_{34}H_{34}Br_2O_6$. Formula weight: 698.41. Temperature: 173(2) K. Wavelength: 1.54178 Å. Orthorhombic, $P2_12_12_1$, crystal size: 0.05 × 0.04 × 0.03 mm^3. Unit cell dimensions: a = 12.1102(4) Å, b = 15.9084(5) Å, c = 16.4050(5) Å, α = 90°, β = 90°, γ = 90°. V = 3160.49(17) $Å^3$, Z = 4, D_{calcd} = 1.468 mg/cm^3. Absorption coefficient: 3.607 mm^{-1}. $F(000)$ = 1386, theta range for data collection: 3.870° to 66.637°, index ranges: $-14 \leq h \leq 14$, $-18 \leq k \leq 18$, $-19 \leq l \leq 19$. Reflections collected 27748, independent reflections 5587 [$R_{(int)}$ = 0.0300]. Completeness to theta = 66.637°, 99.9%. Largest diff. peak and hole 0.001 and 0.000 e.$Å^{-3}$. Refinement method was Full-matrix least-squares on F^2, with Goodness-of-fit on F^2 = 0.676. Data / restraints / parameters: 5587 / 0 / 384. Final R indices [$I > 2\sigma(I)$]: R_1 = 0.0229, wR_2 = 0.0751, R indices (all data): R_1 = 0.0251, wR_2 = 0.0785. Flack parameter −0.002(5).

Crystallographic data for **1a** has been deposited at the Cambridge Crystallographic Data Centre (Deposition number CCDC 1823682). Copies of these data can be obtained free of charge via www.ccdc.cam.ac.uk/conts/retrieving.html or from the Cambridge Crystallographic Data Centre, 12, Union Road, Cambridge CB21EZ, UK. [Fax: (+44) 1223-336-033; or email: deposit@ccdc.cam.ac.uk].

ECD calculation

The conformations generated by BALLOON were subjected to semiempirical PM3 quantum mechanical geometry optimizations using the Gaussian 09 program (Gaussian, Inc., Pittsburgh, PA, 2009). Duplicate conformations were identified and removed when the root-mean-square (RMS) distance was less than 0.5 Å for any two geometry optimized conformations. There maining conformations were further optimized at the B3LYP/6-31G* level of theory in MeOH with the IEFPCM solvation model using Gaussian 09, and the duplicate conformations emerging after these calculations were removed according to the same RMS criteria above. The harmonic vibrational frequencies were calculated to confirm the stability of the final conformers. The oscillator strengths and rotational strengths of the 20 weakest electronic excitations of

each conformer were calculated using the TDDFT methodology at the B3LYP/6-311G** level of theory with MeOH as the solvent with the IEFPCM solvation model implemented in Gaussian 09. The ECD spectra for each conformer were simulated using a Gaussian function with a band widths of 0.45eV. The spectra were combined after Boltzmann weighting according to their population contributions.

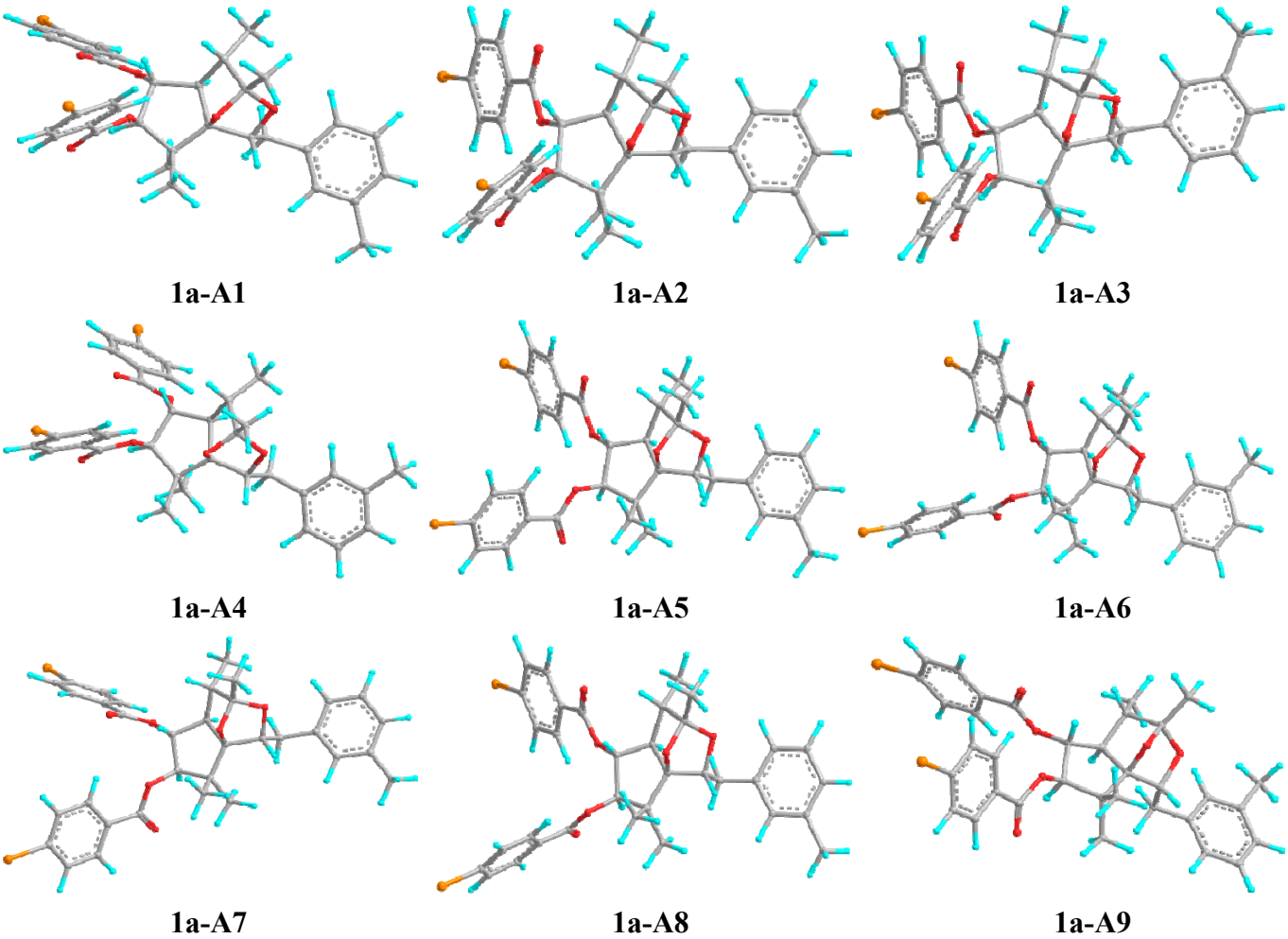

Figure S10. Optimized geometries of predominant conformers of **1a-A** at the B3LYP/6-31G(d,p) level in the gas phase.

Table S3. Conformational analysis of **1a-A**.

Conformation	SCF	G[a]	U[b]	ΔE[c]	Ratio (%)[d]
1a-A1	−6916.25	0.533189	0.652452	0	19.98
1a-A2	−6916.25	0.53393	0.652475	0.0753	17.60
1a-A3	−6916.25	0.533747	0.652541	0.0816	17.41
1a-A4	−6916.25	0.533226	0.652561	0.0879	17.23
1a-A5	−6916.25	0.534274	0.652697	0.615	7.08
1a-A6	−6916.25	0.532248	0.652476	0.6903	6.23

1a-A7	−6916.25	0.53247	0.652578	0.7844	5.32
1a-A8	−6916.25	0.532097	0.652594	0.8409	4.83
1a-A9	−6916.25	0.533655	0.652596	0.935	4.12
1a-A10	−6916.25	0.533403	0.652688	3.1501	0.10
1a-A11	−6916.25	0.534224	0.652797	3.1689	0.09

[a]Gibbs free energy in kcal/mol. [b]Internal energy in kcal/mol. [c]Relative energy in kcal/mol. [d]Conformational distribution calculated by using the respective parameters above at B3LYP/6-31G(d,p) level in the gas phase. T=298 K

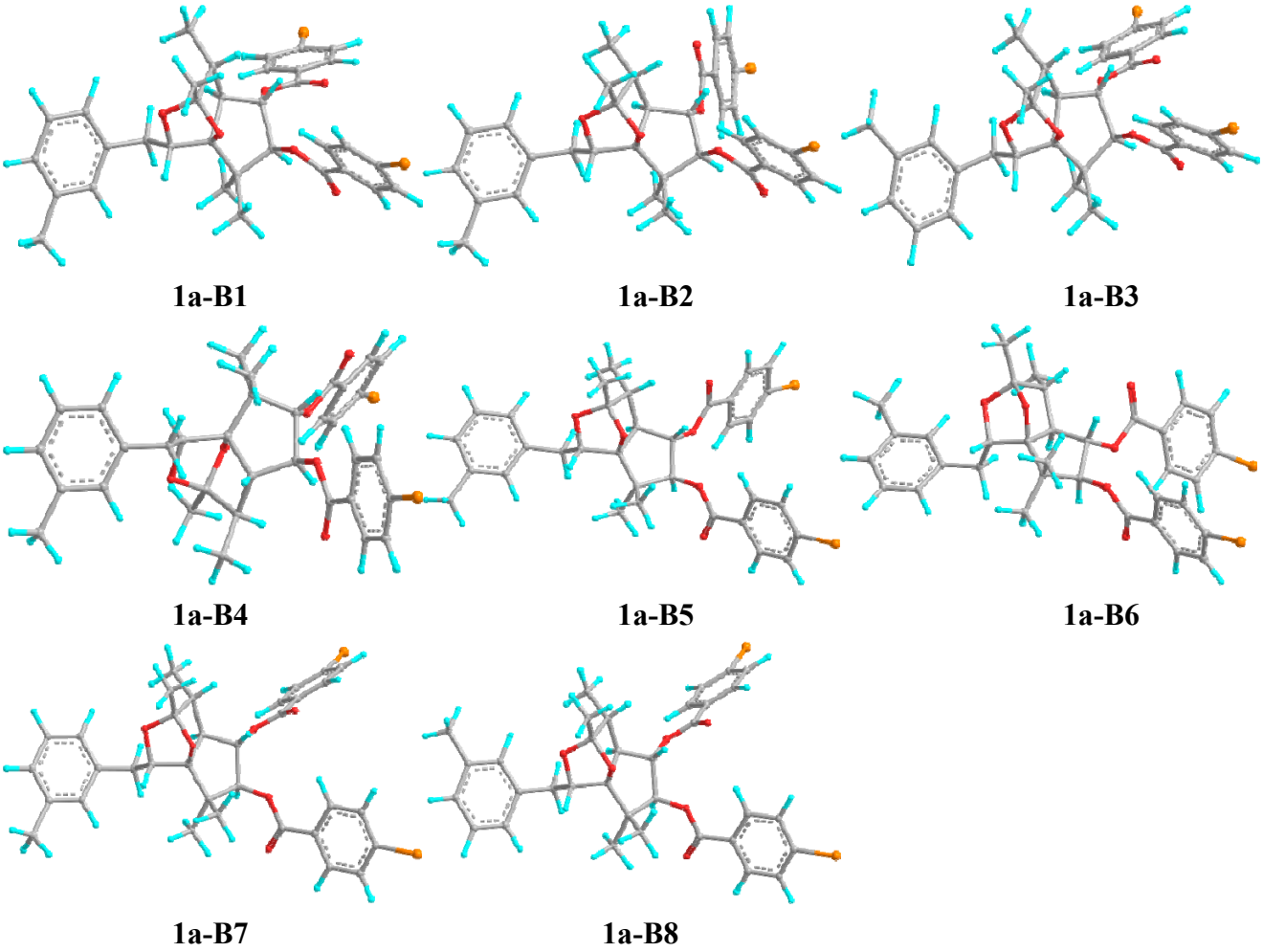

Figure S11. Optimized geometries of predominant conformers of **1a-B** at the B3LYP/6-31G(d,p) level in the gas phase.

Table S4. Conformational analysis of **1a-B**.

Conformation	SCF	G[a]	U[b]	ΔE[c]	Ratio (%)[d]
1a-B1	−6916.254386	0.533307	0.652456	0	21.02
1a-B2	−6916.254283	0.53393	0.652475	0.0753	18.51
1a-B3	−6916.25437	0.533325	0.652559	0.0753	18.51

1a-B4	−6916.254338	0.533923	0.652549	0.0879	18.12
1a-B5	−6916.253644	0.534262	0.652696	0.615	7.44
1a-B6	−6916.253275	0.532524	0.652497	0.7216	6.22
1a-B7	−6916.253289	0.531488	0.652568	0.7593	5.83
1a-B8	−6916.253037	0.533668	0.652596	0.935	4.34

[a]Gibbs free energy in kcal/mol. [b]Internal energy in kcal/mol. [c]Relative energy in kcal/mol. [d]Conformational distribution calculated by using the respective parameters above at B3LYP/6-31G(d,p) level in the gas phase. T=298 K

PTP1B Inhibitory Bioassay.

Recombinant human PTP1B was purchased from SIGMA-ALDRICH. And the reagent 4-nitrophenyl phosphate disodium salt (*p*NPP) was applied as a substrate for the assessment of PTP1B activity. PTP1B protein was dissolved in enzyme dilution buffer (50 mmol/L 3-[*N*-morpholino] propanesulfonic acid (Mops), 1 mM EDTA, and 1 mM dithiothreitol, 1 mg/mL BSA, pH 6.5), and inhibitors were pre-incubated with the recombinant human PTP1B at 37 °C for 30 min. The bioassay was performed in a reaction mixture containing 15 nmol/L recombinant PTP1B, 10 mM *p*NPP, 1 mM EDTA, 1 mM dithiothreitol, and 1 mg/mL BSA, in 50 mmol/L Mops, pH 6.5, incubated at 37 °C for 45 min in a 96-well plate (100 μL per well), and the reaction was terminated by addition of 50 μL 3 M NaOH each well. Oleanolic acid was used as the positive control, a similar system without samples was applied as the negative control, and parallel experiments without PTP1B protein and samples were utilized as the blank control. Dephosphorylation of *p*NPP could generate product *p*-nitrophenol (*p*NP), which could be monitored at an absorbance of 405 nm by microplate reader (read every 5 min for 30 min) and the slope of the initial rate for the kinetic curve in each well was applied to determine the activity of PTP1B. Samples with good inhibition rate (>50% at 200 μM) were tested for further determination of IC_{50} values. Mollebenzylanols A (**1**) and B (**2**), and rhodojaponin III (**3**), **1a** as well as oleanolic acid exhibited 75.4%, 70.5%, 23.4%, 3.4%, 90.6%, and 99.2% inhibitory ratio against PTP1B protein at final concentration of 200 μM, respectively. Then, PTP1B inhibitory activity of mollebenzylanols A (**1**) and B (**2**), **1a**, and the positive control oleanolic acid were tested under different dosages. The IC_{50} value (50% percentage inhibition concentration) was calculated with Origin 8.0 software from the non-linear curve fitting of the percentage of inhibition (% inhibition) versus logarithm of the inhibitor concentration [I] by using the following equation: % Inhibition = $100/(1+[IC_{50}/10^{[I]}]^{k})$, where k is the Hill coefficient.

Molecular Docking Study.

Molecular docking simulation of five inhibitors (compounds **1−3**, **1a**, and oleanolic acid) to human PTP1B were performed by the LibDock protocol of Discovery Studio 2.5 (BIOVIA, San Diego, CaA). PTP1B X-ray crystal structure at 1.5 Å resolution (PDB ID: 2hb1) was taken from RCSB Protein Data Bank (www.rcsb.org). The structure was protonated and deleted water at pH 7 using Clean Protein tool in Discovery Studio 2.5. The 3D structures of the inhibitors were prepared through Sybyl-X 2.0 (Tripos Inc., St. Louis, MO), and tripos force field was utilized for energy minimization of molecules **1−3** and **1a** with a root-mean-square (RMS) gradient of 0.01 kcal/mol·Å. The Generalized Born with Molecular Volume (GBMV) method was used for implicit solvent model. All residues within 20 Å from the sulfur atom of the catalytic cysteine residue (Cys215) were defined as a docking site. The number of docking runs was set to 100 for each inhibitor. All other parameters were set as default. Energy minimization for the protein in complex with the inhibitor was then conducted to remove energetically unfavorable contacts with the same parameters as mentioned above. The energy parameters between the enzyme and five inhibitors were calculated by Autodock 4.2.6.[1]

[1] Morris, G. M.; Huey, R.; Lindstrom, W.; Sanner, M. F.; Belew, R. K.; Goodsell, D. S.; Olson, A. J. *J. Comput. Chem.* **2009**, *30*, 2785.

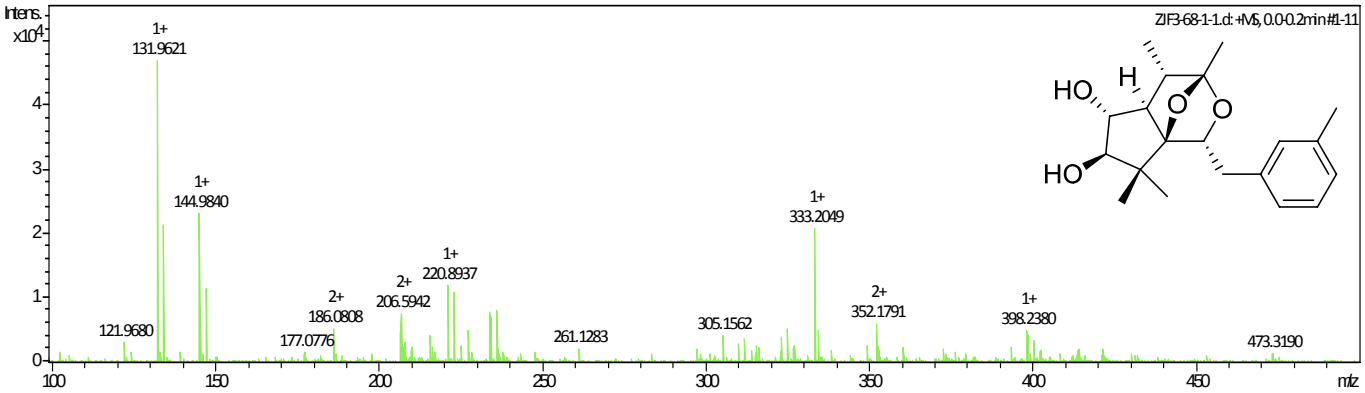

Figure S12. HR-ESI-MS spectrum of **1.**

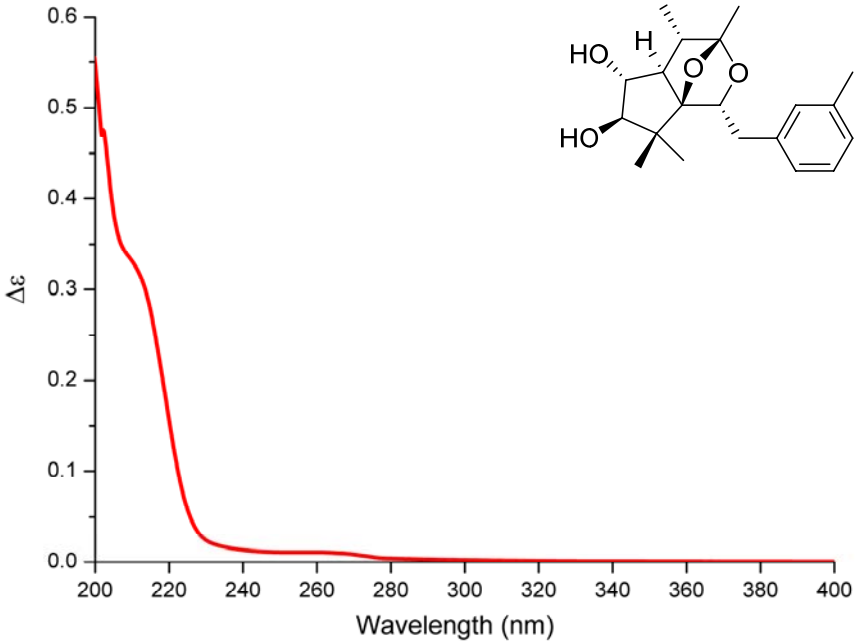

Figure S13. UV spectrum of **1** in methanol.

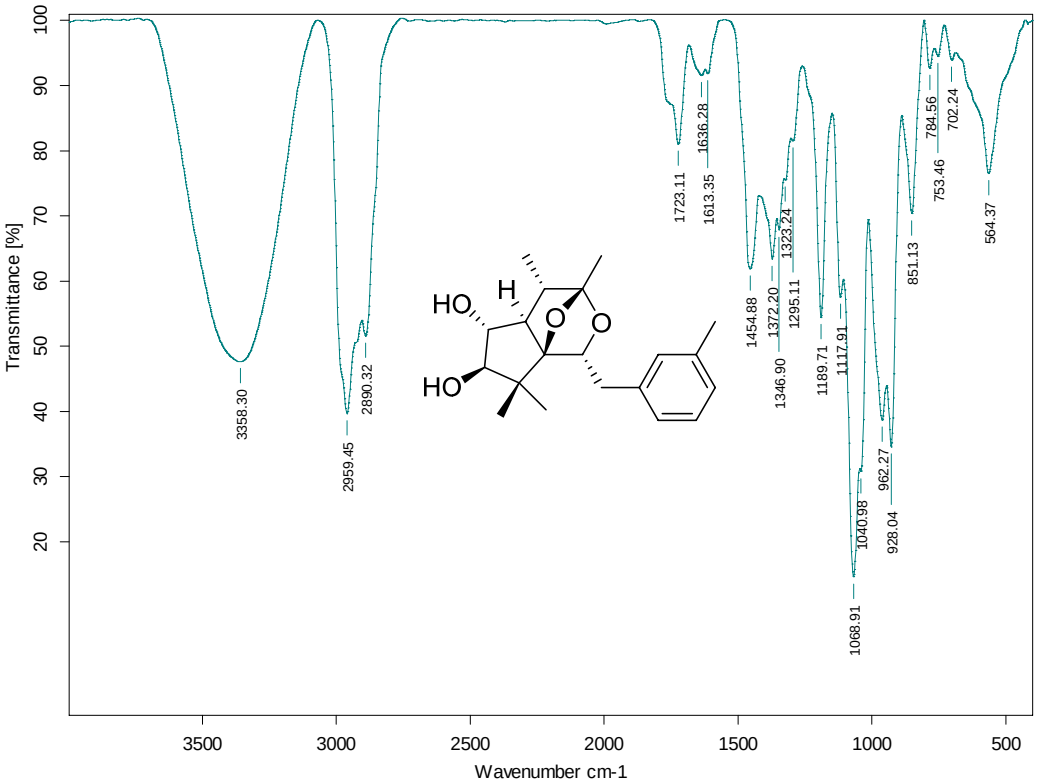

Figure S14. IR spectrum of **1** (KBr)

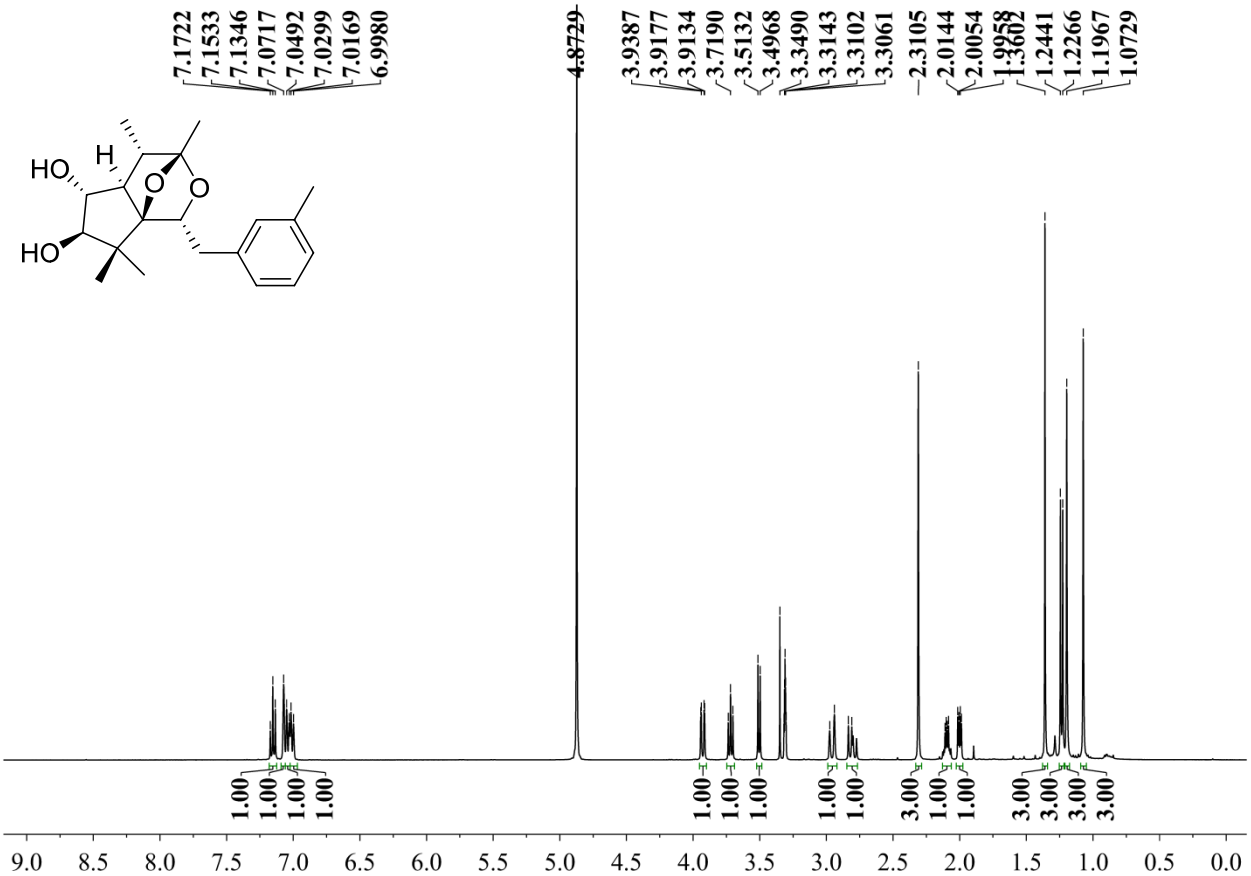

Figure S15. ^{1}H NMR spectrum of **1** (400 MHz, methanol-d_4)

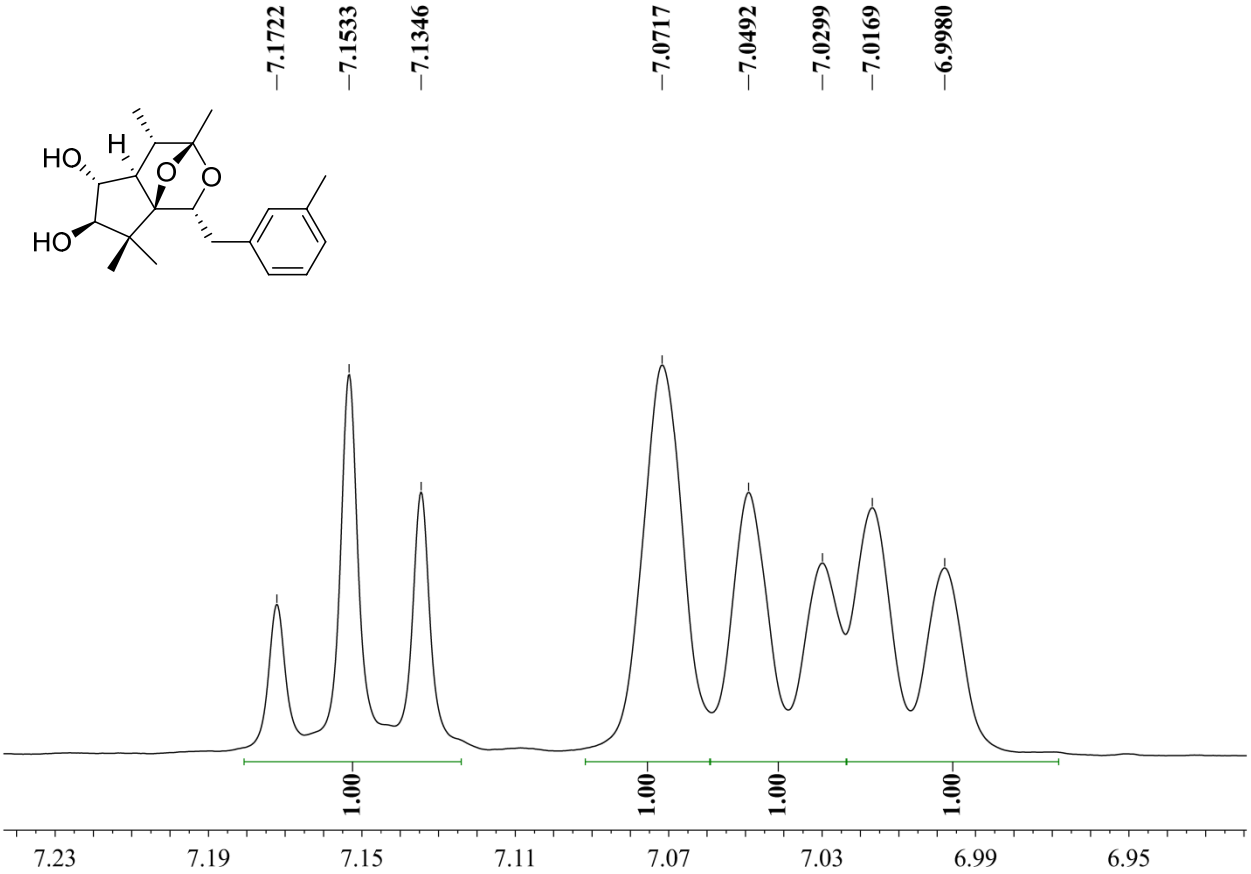

Figure S16. ^{1}H NMR spectrum (amplified) of **1** (400 MHz, methanol-d_4)

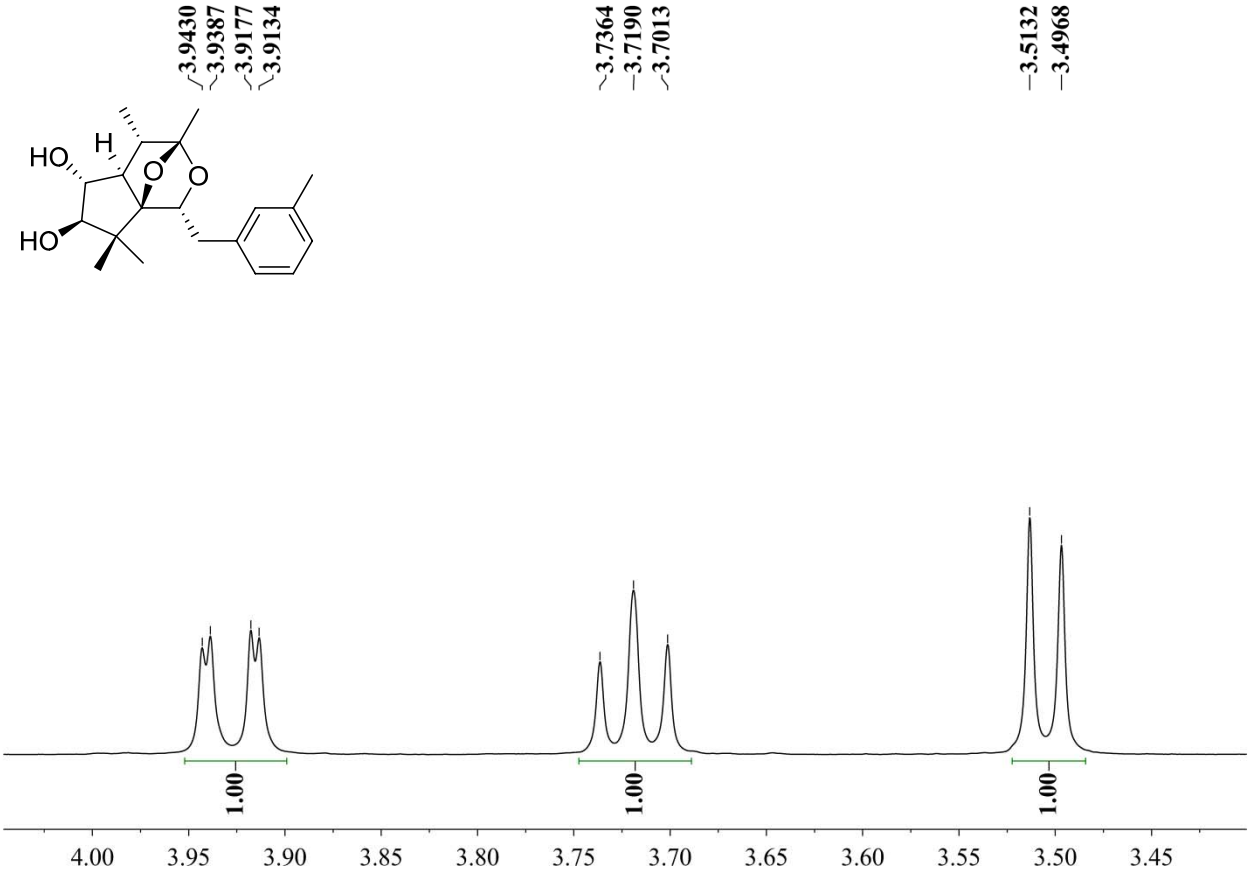

Figure S17. ^{1}H NMR spectrum (amplified) of **1** (400 MHz, methanol-d_4)

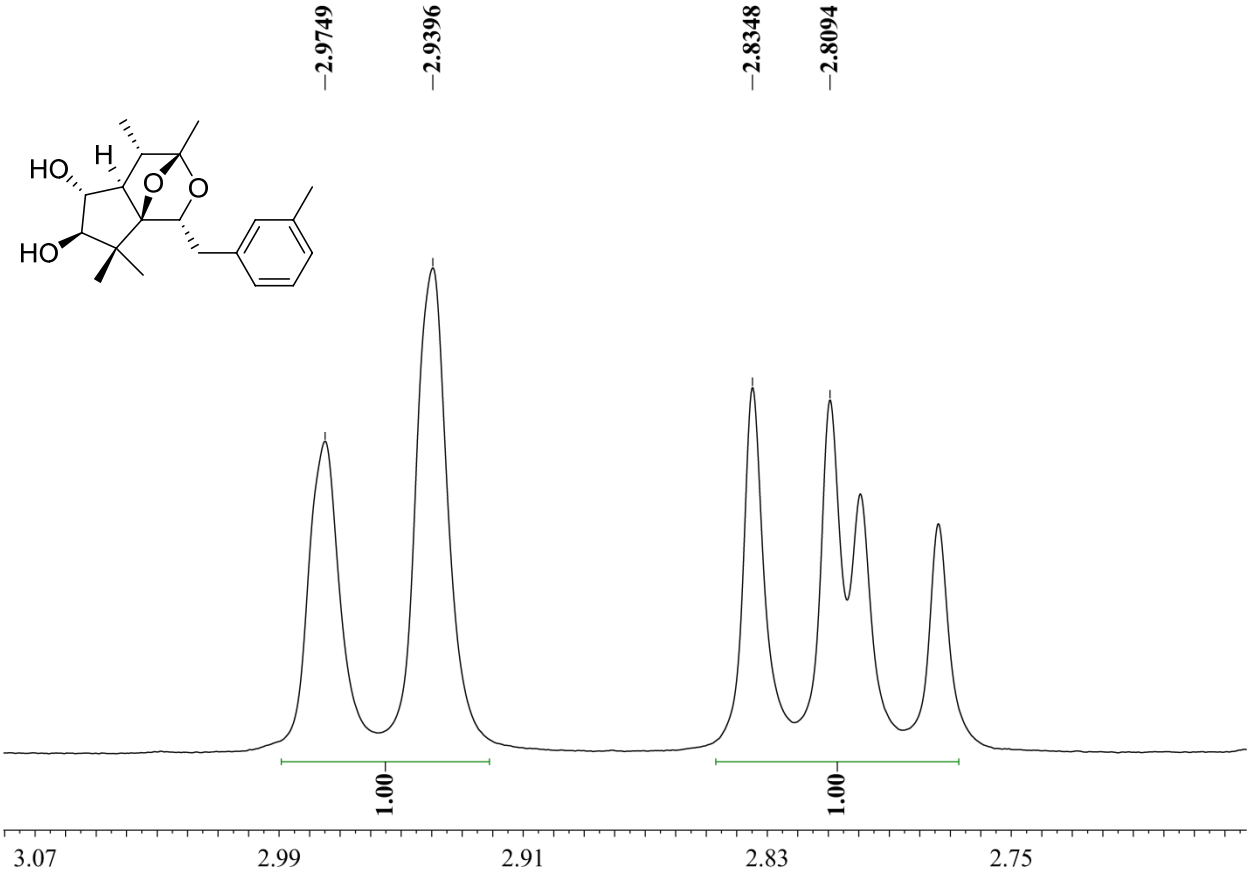

Figure S18. ^{1}H NMR spectrum (amplified) of **1** (400 MHz, methanol-d_4)

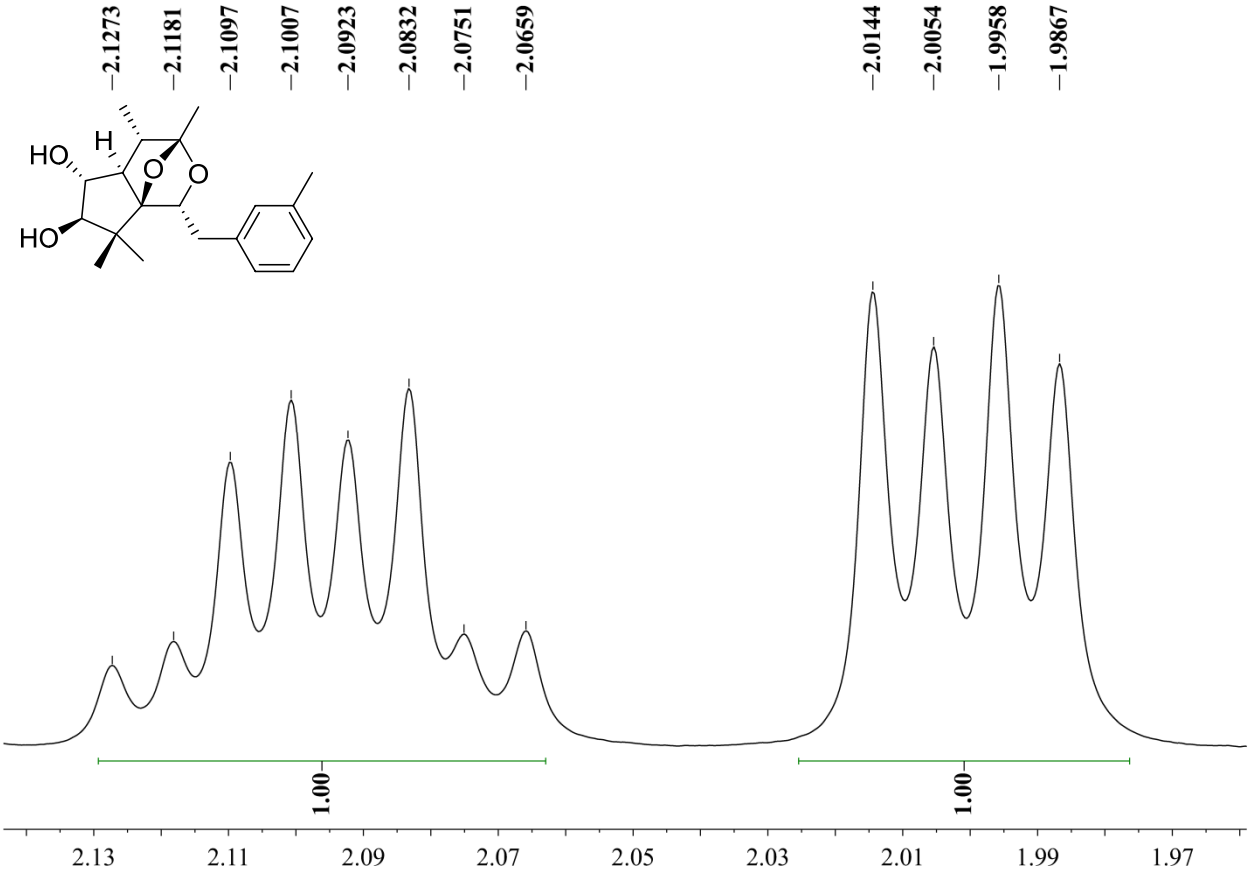

Figure S19. ^{1}H NMR spectrum (amplified) of **1** (400 MHz, methanol-d_4)

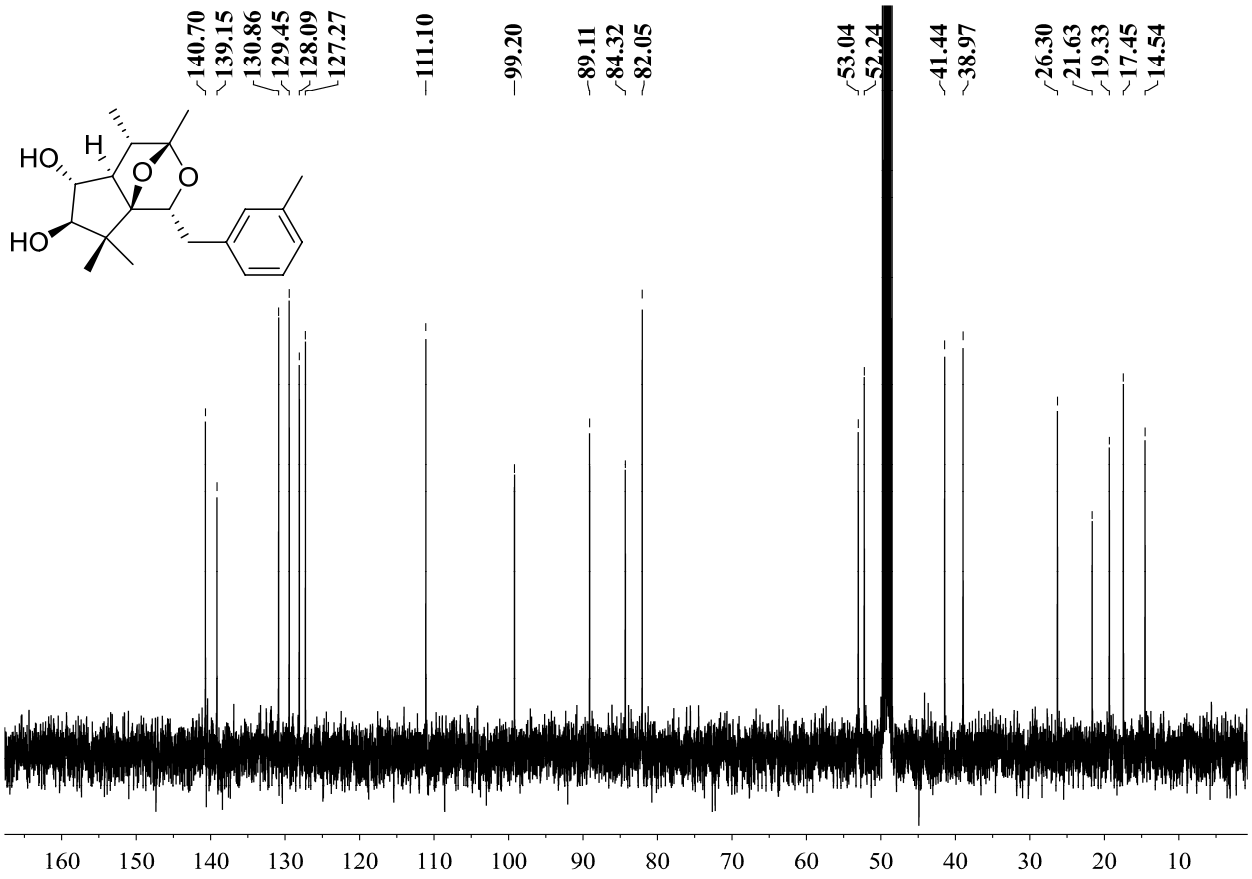

Figure S20. ^{13}C NMR spectrum of **1** (100 MHz, methanol-d_4)

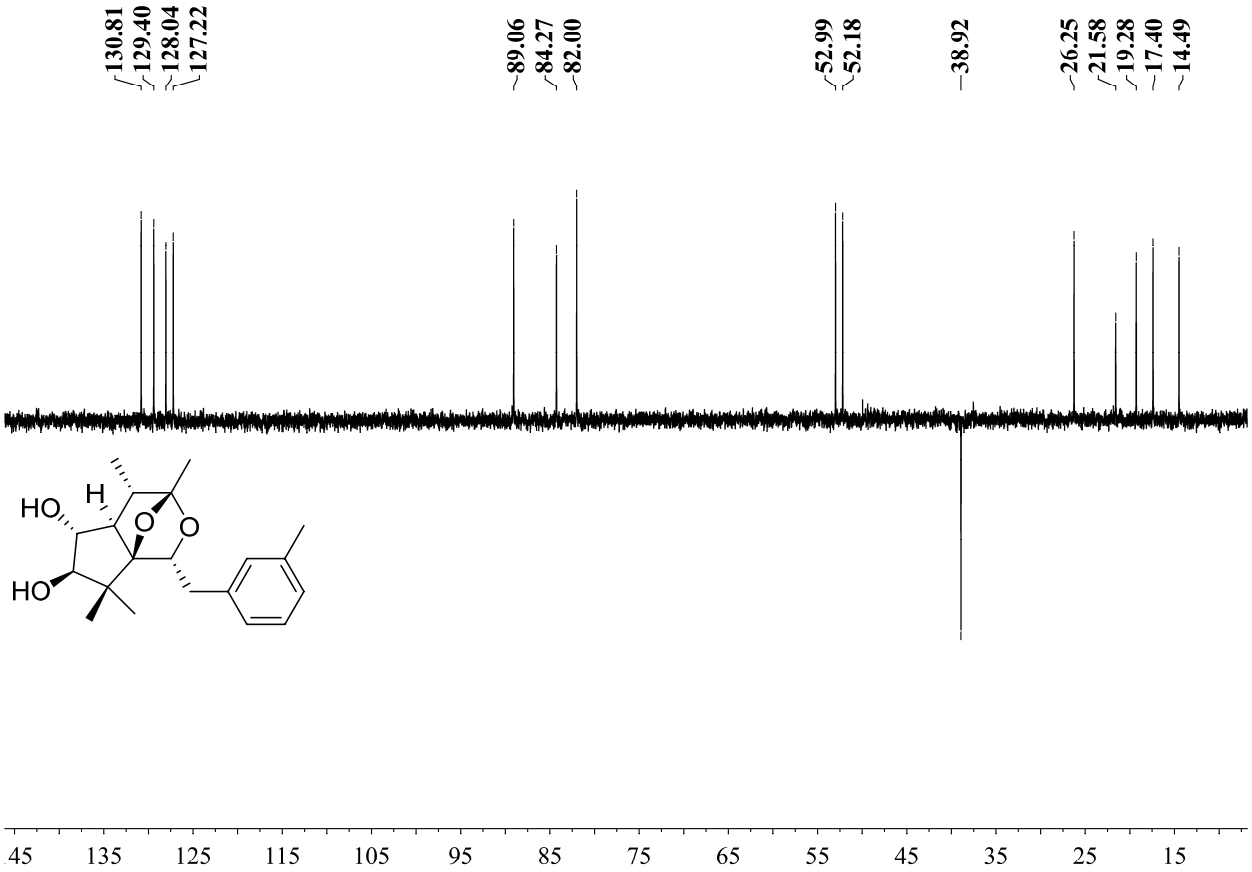

Figure S21. DEPT spectrum of **1** (100 MHz, methanol-d_4)

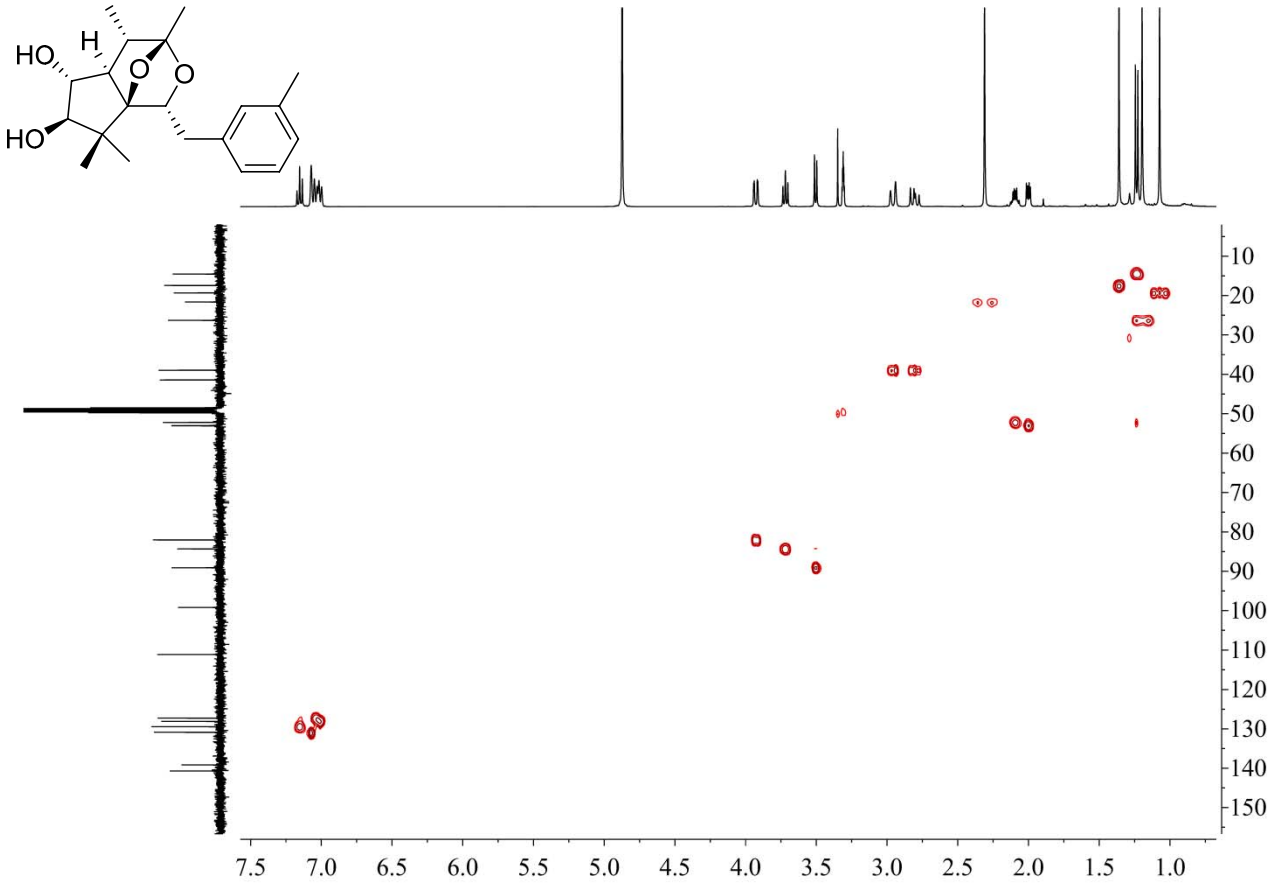

Figure S22. HSQC spectrum of **1** (^{1}H: 400 MHz, ^{13}C: 100 MHz, methanol-d_4)

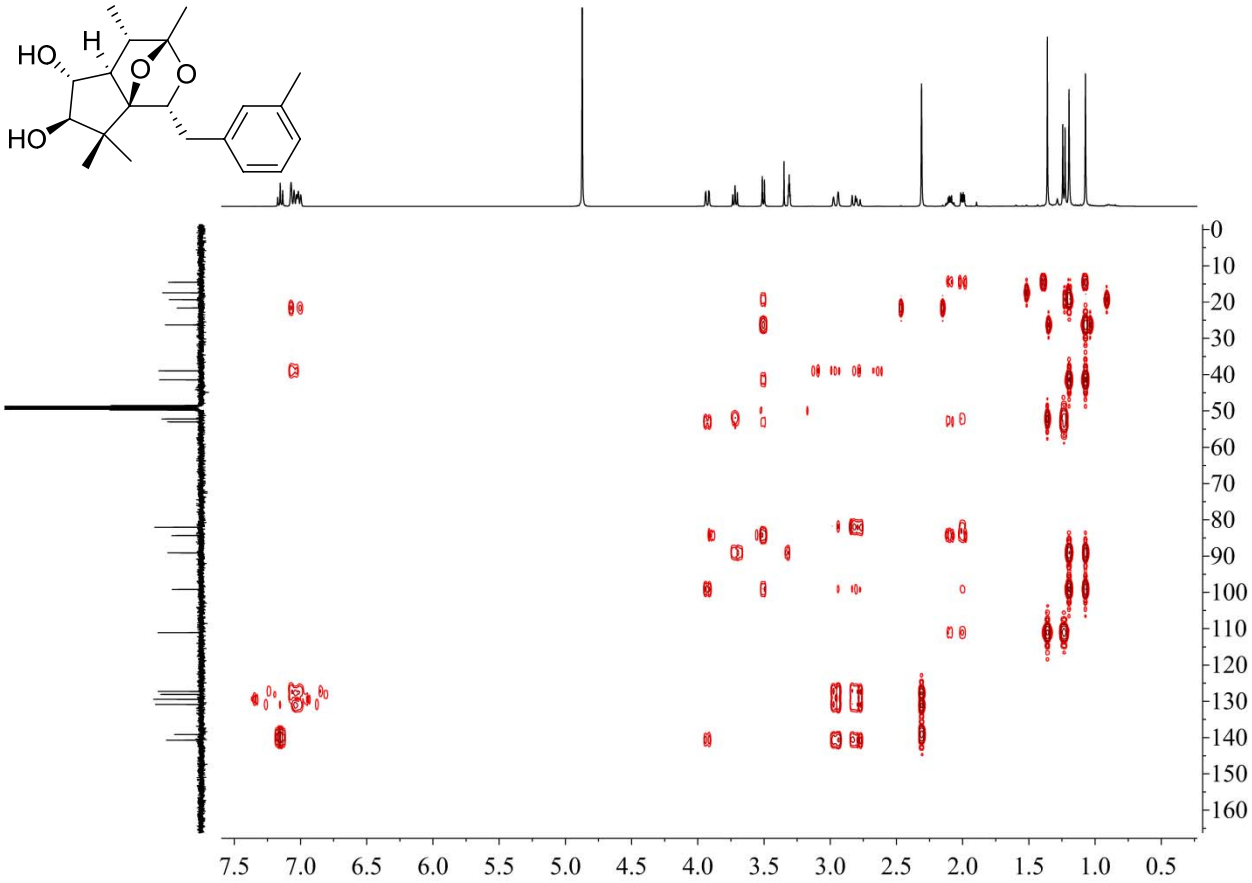

Figure S23. HMBC spectrum of **1** (^{1}H: 400 MHz, ^{13}C: 100 MHz, methanol-d_4)

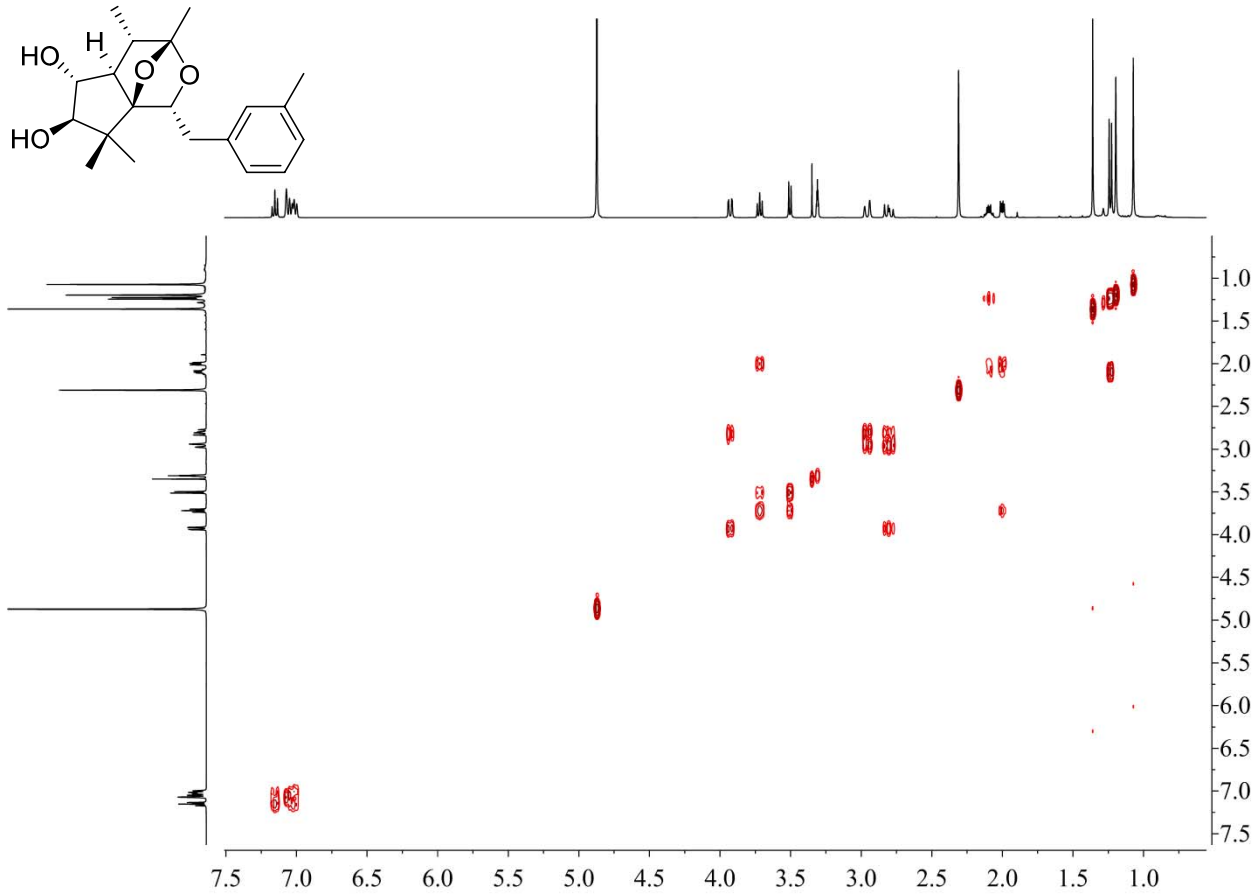

Figure S24. ^{1}H–^{1}H COSY spectrum of **1** (400 MHz, methanol-d_4)

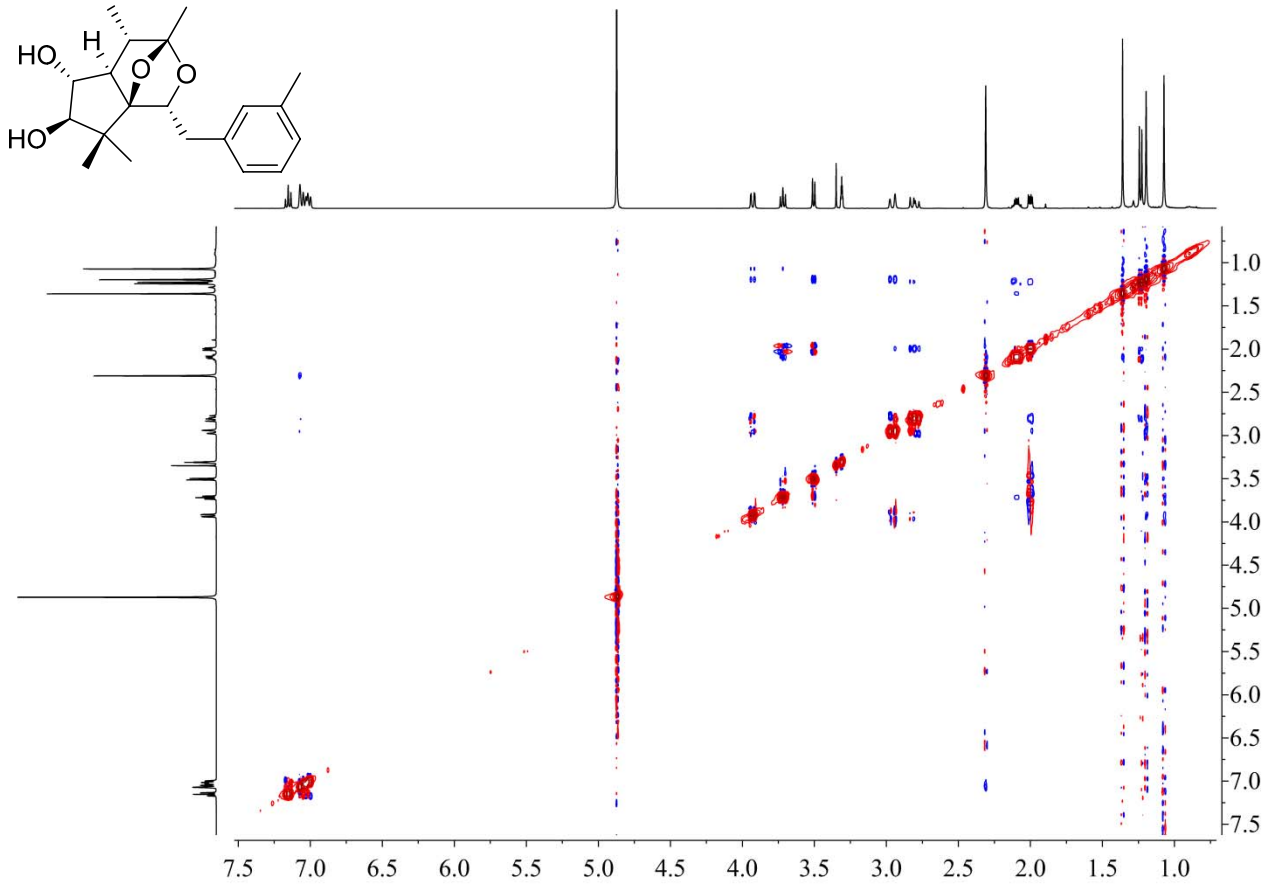

Figure S25. NOESY spectrum of **1** (400 MHz, methanol-d_4)

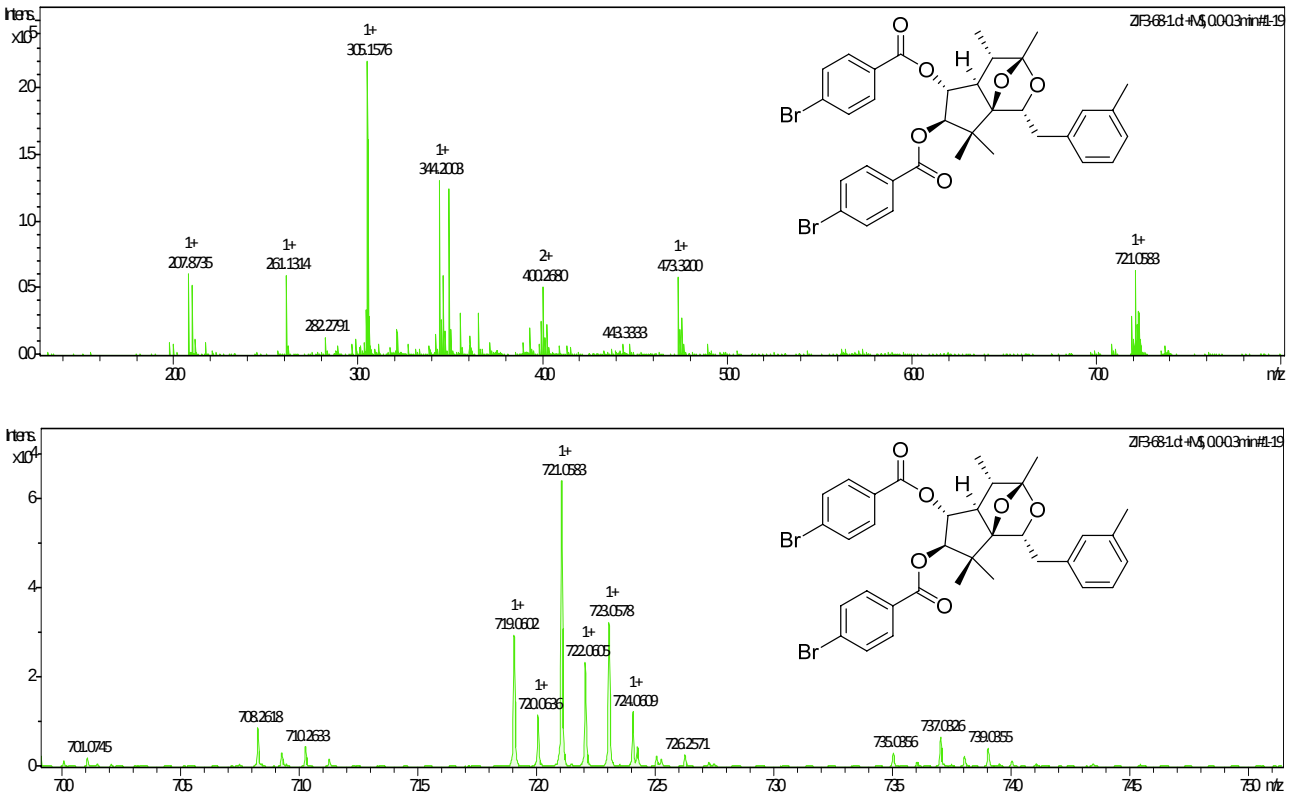

Figure S26. HR-ESI-MS spectrum of **1a**.

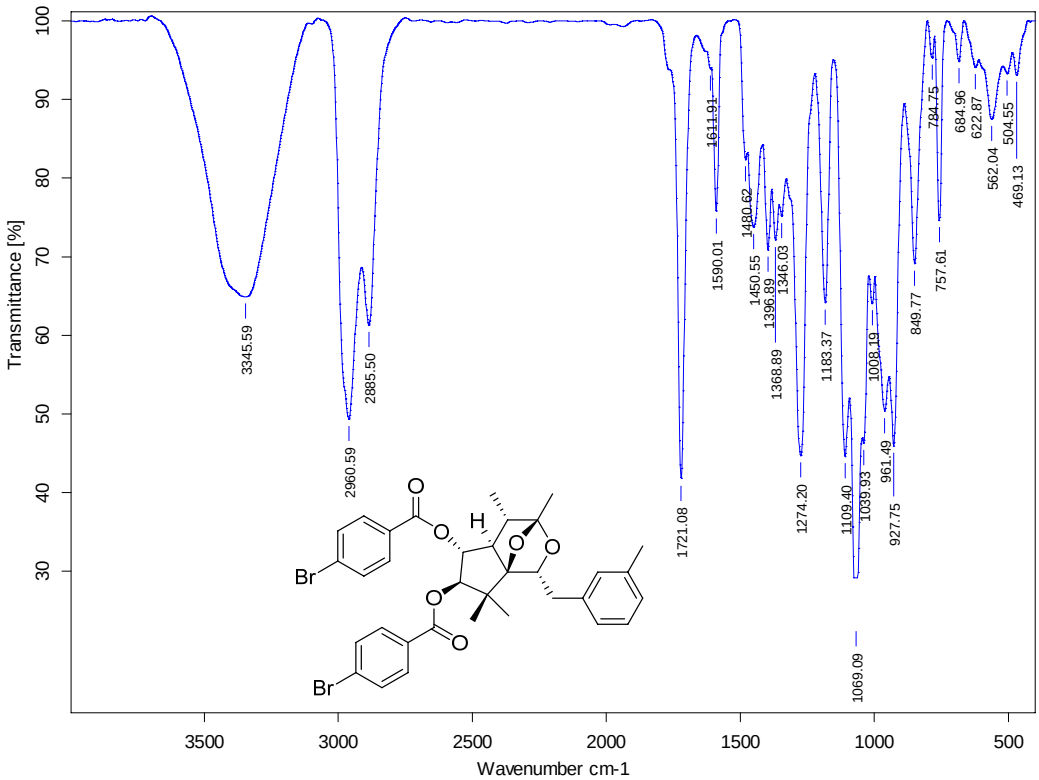

Figure S27. IR spectrum of **1a** (KBr)

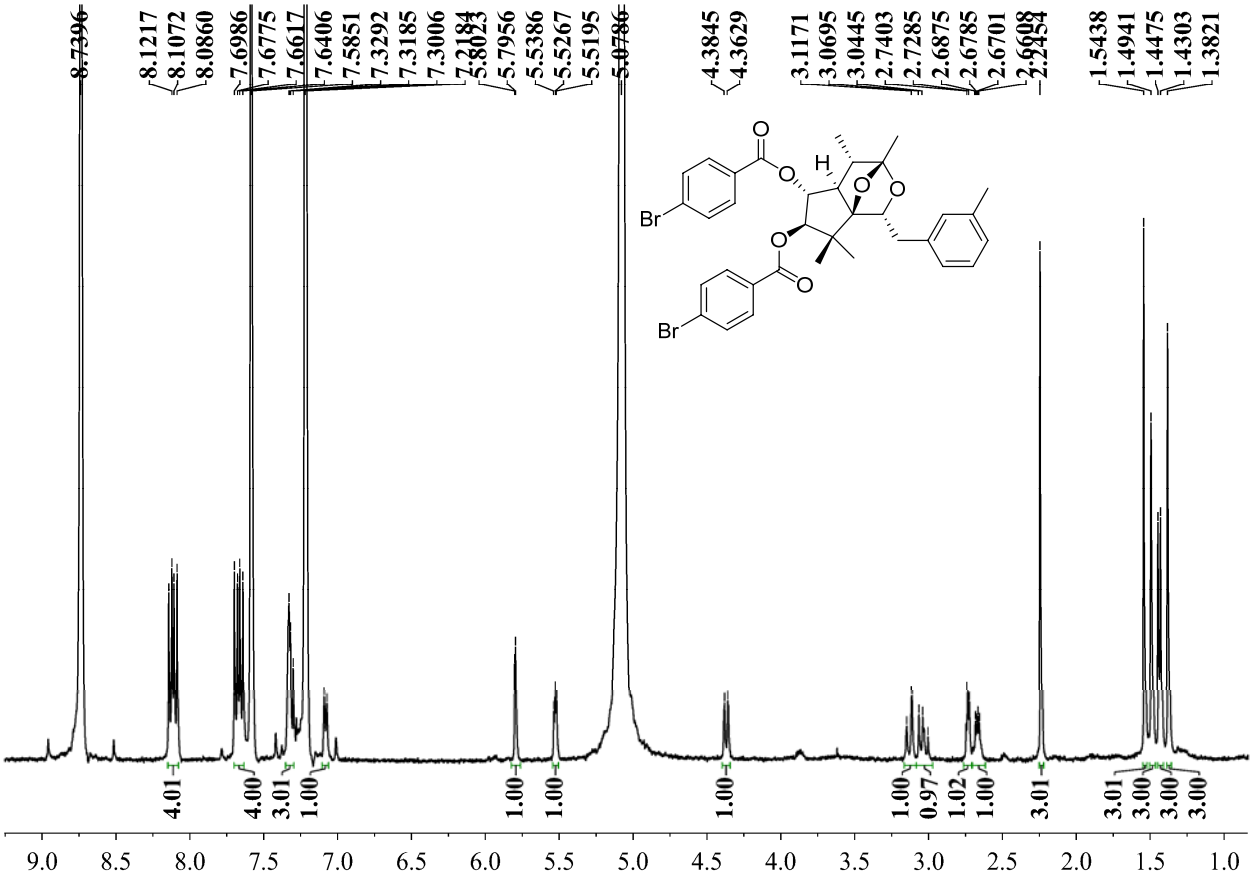

Figure S28. ^{1}H NMR spectrum of **1a** (400 MHz, pyridine-d_5)

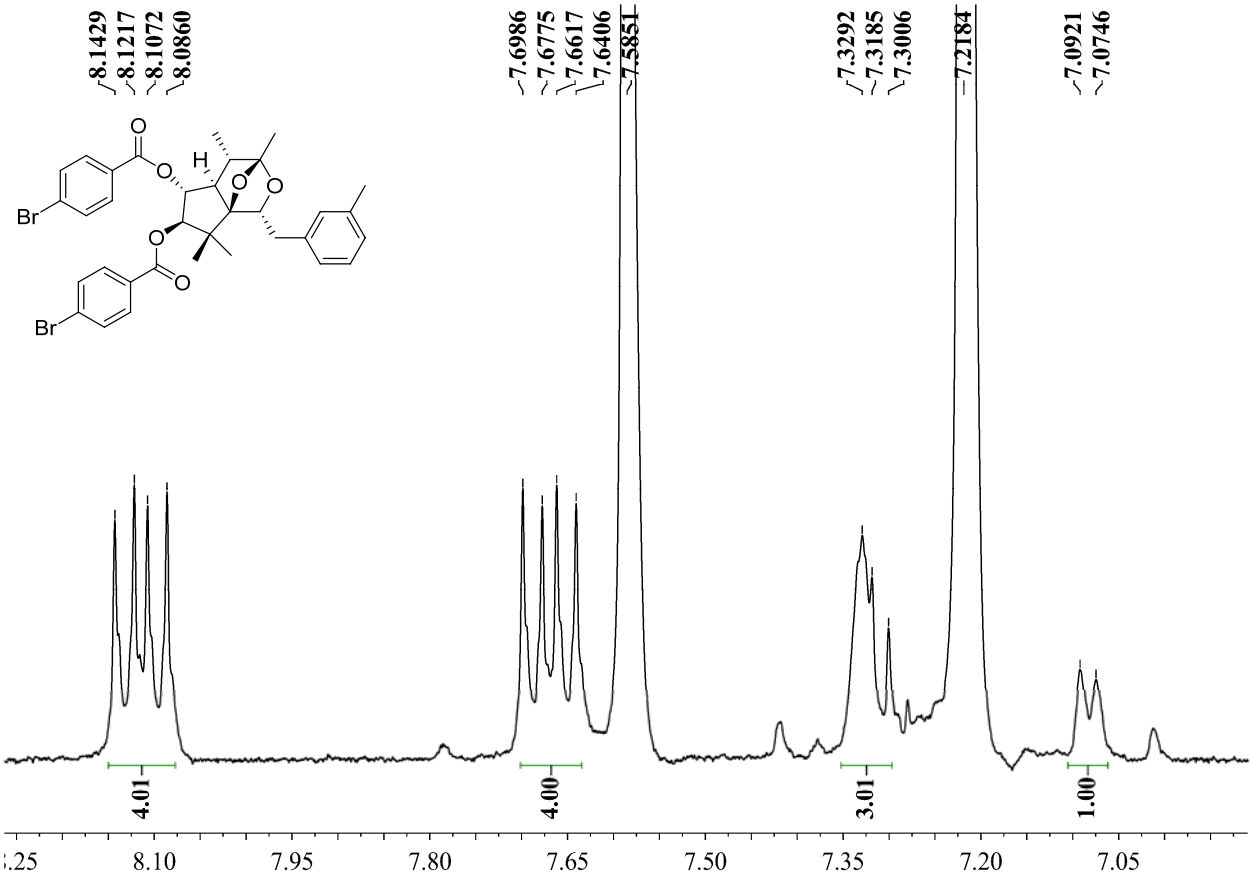

Figure S29. ^{1}H NMR spectrum (amplified) of **1a** (400 MHz, pyridine-d_5)

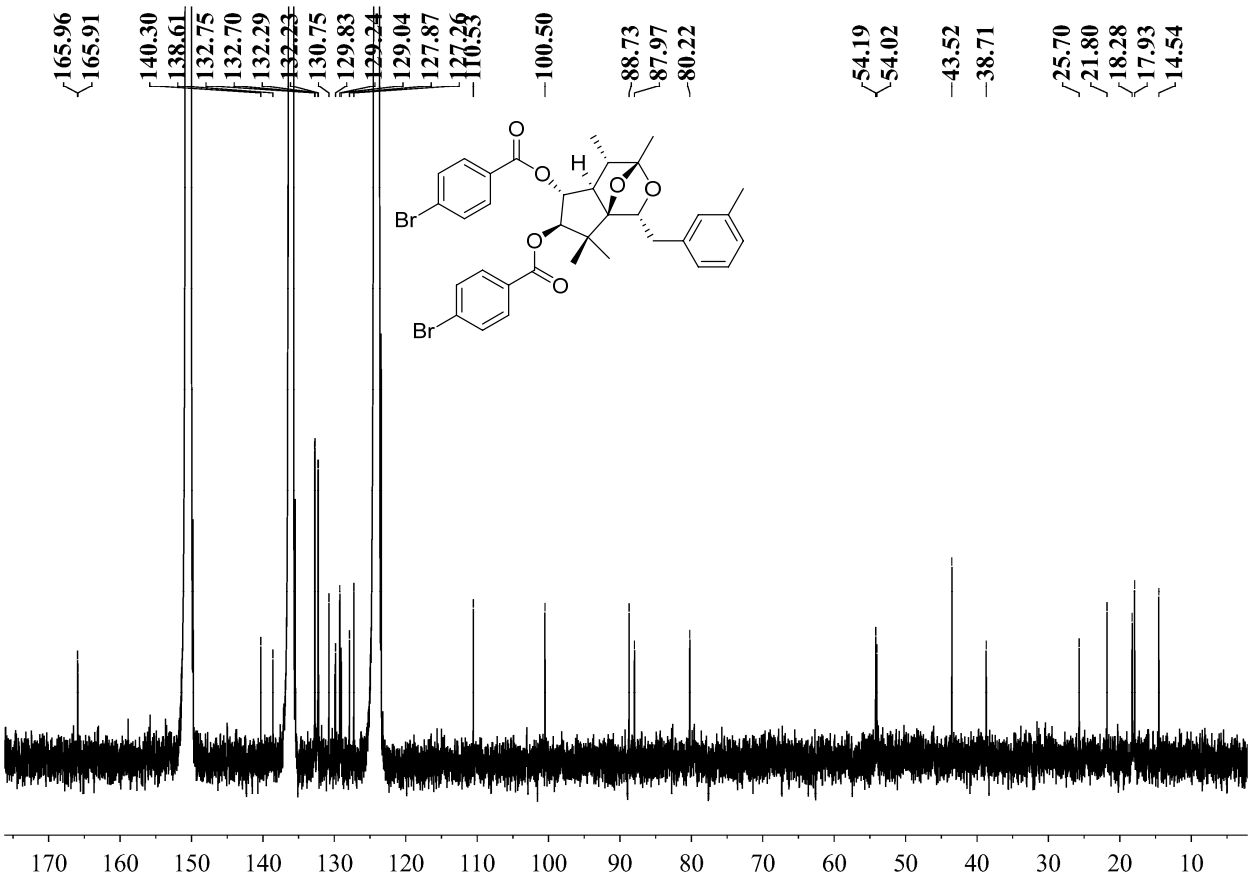

Figure S30. ^{13}C NMR spectrum of **1a** (100 MHz, pyridine-d_5)

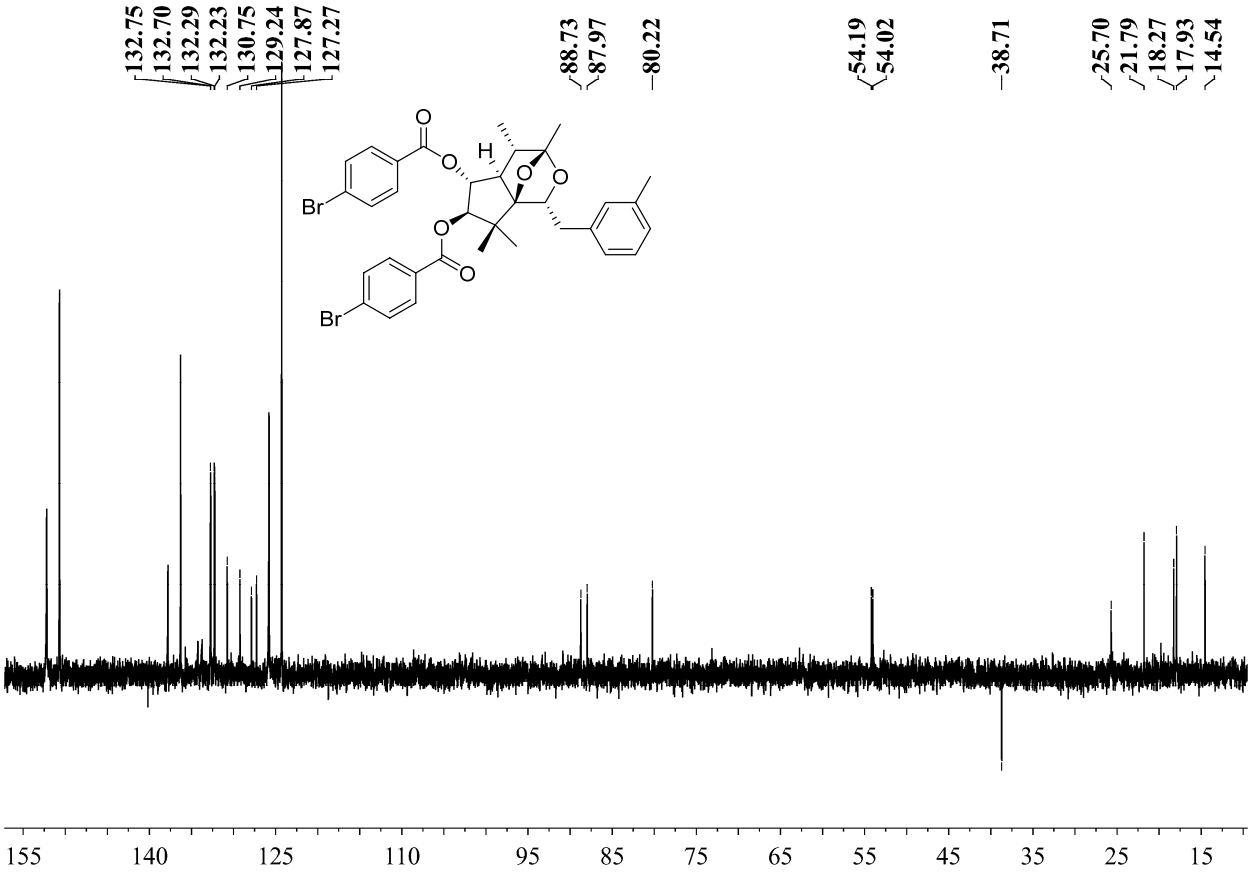

Figure S31. DEPT spectrum of **1a** (100 MHz, pyridine-d_5)

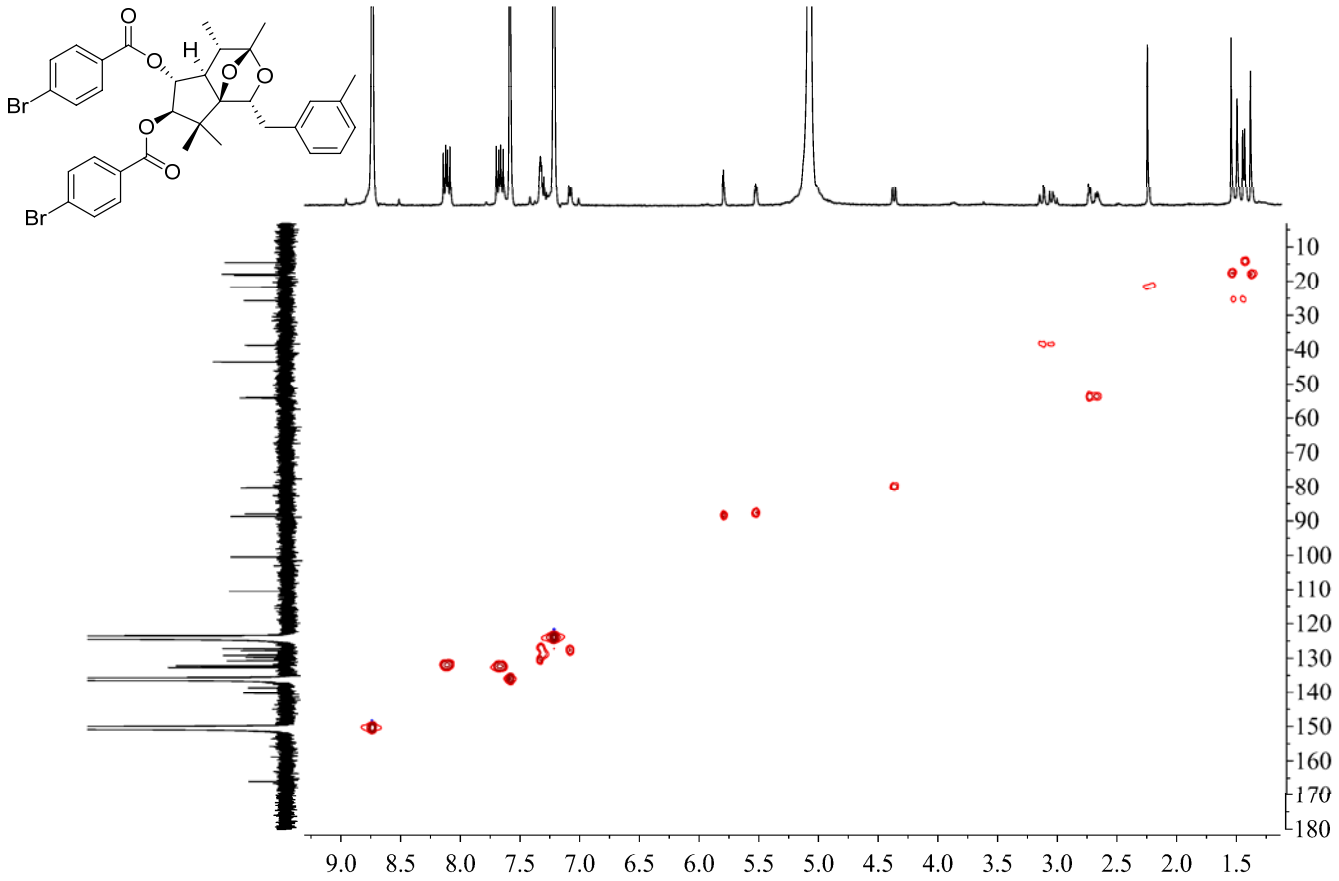

Figure S32. HSQC spectrum of **1a** (^{1}H: 400 MHz, ^{13}C: 100 MHz, pyridine-d_5)

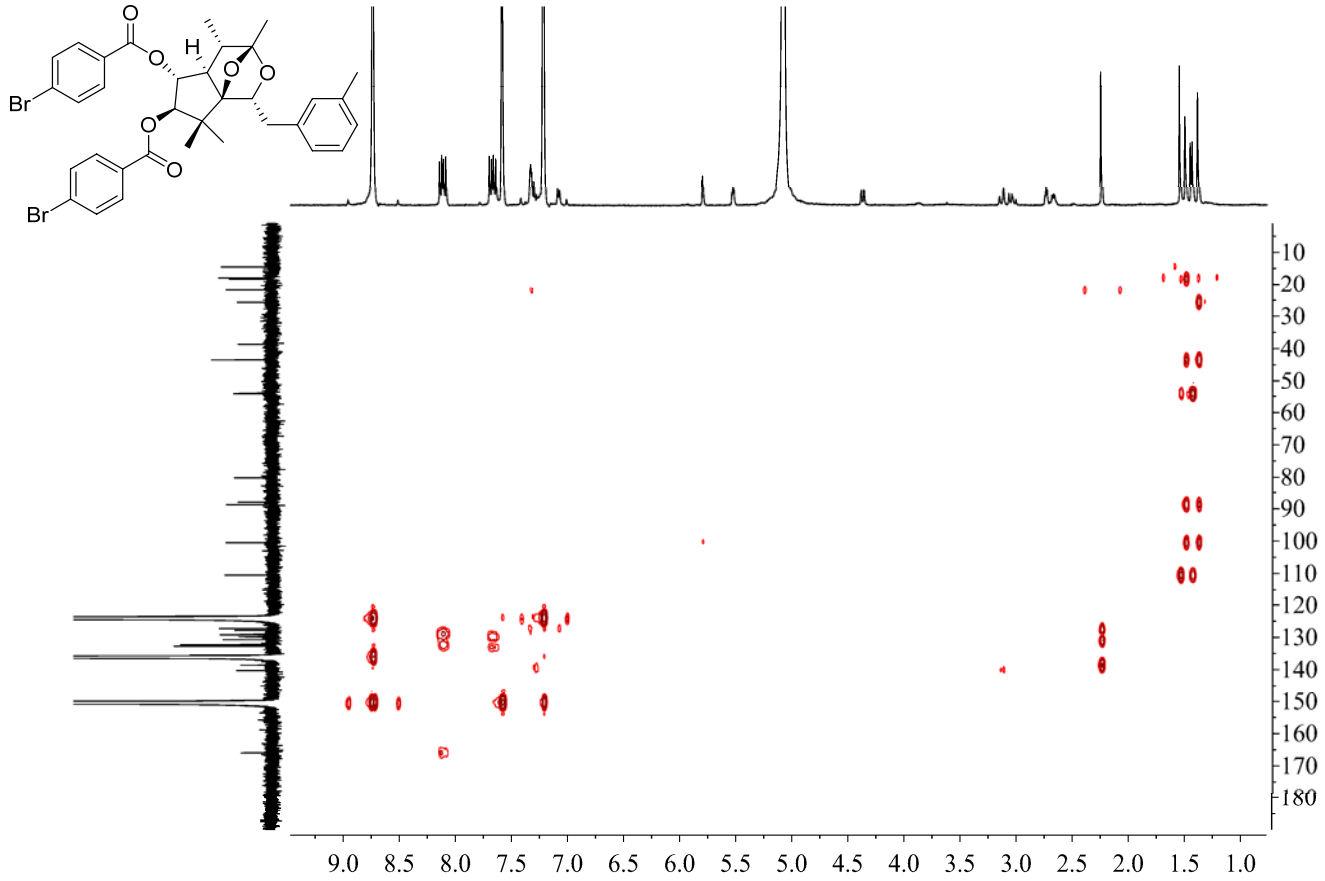

Figure S33. HMBC spectrum of **1a** (^{1}H: 400 MHz, ^{13}C: 100 MHz, pyridine-d_5)

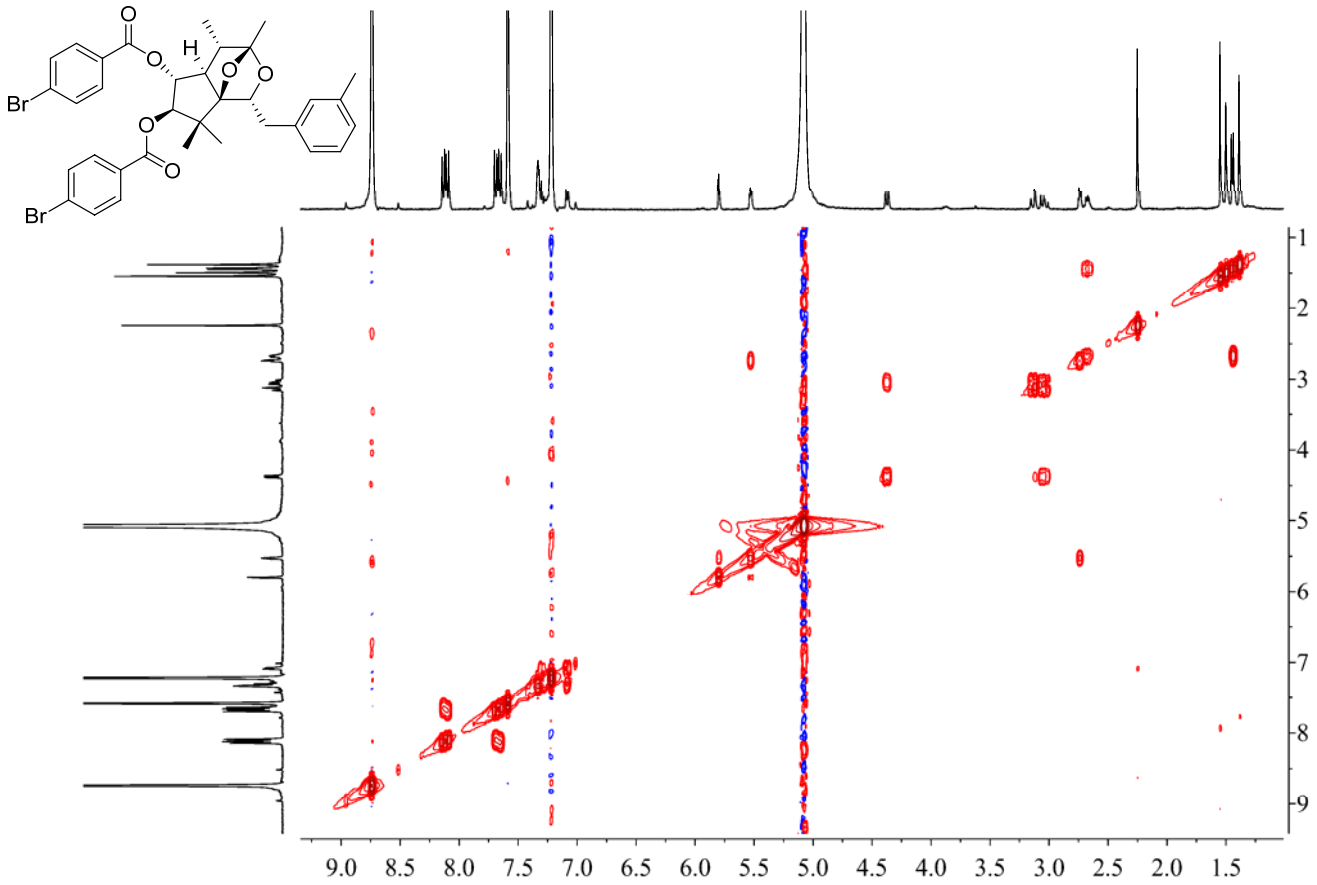

Figure S34. ^{1}H–^{1}H COSY spectrum of **1a** (400 MHz, pyridine-d_5)

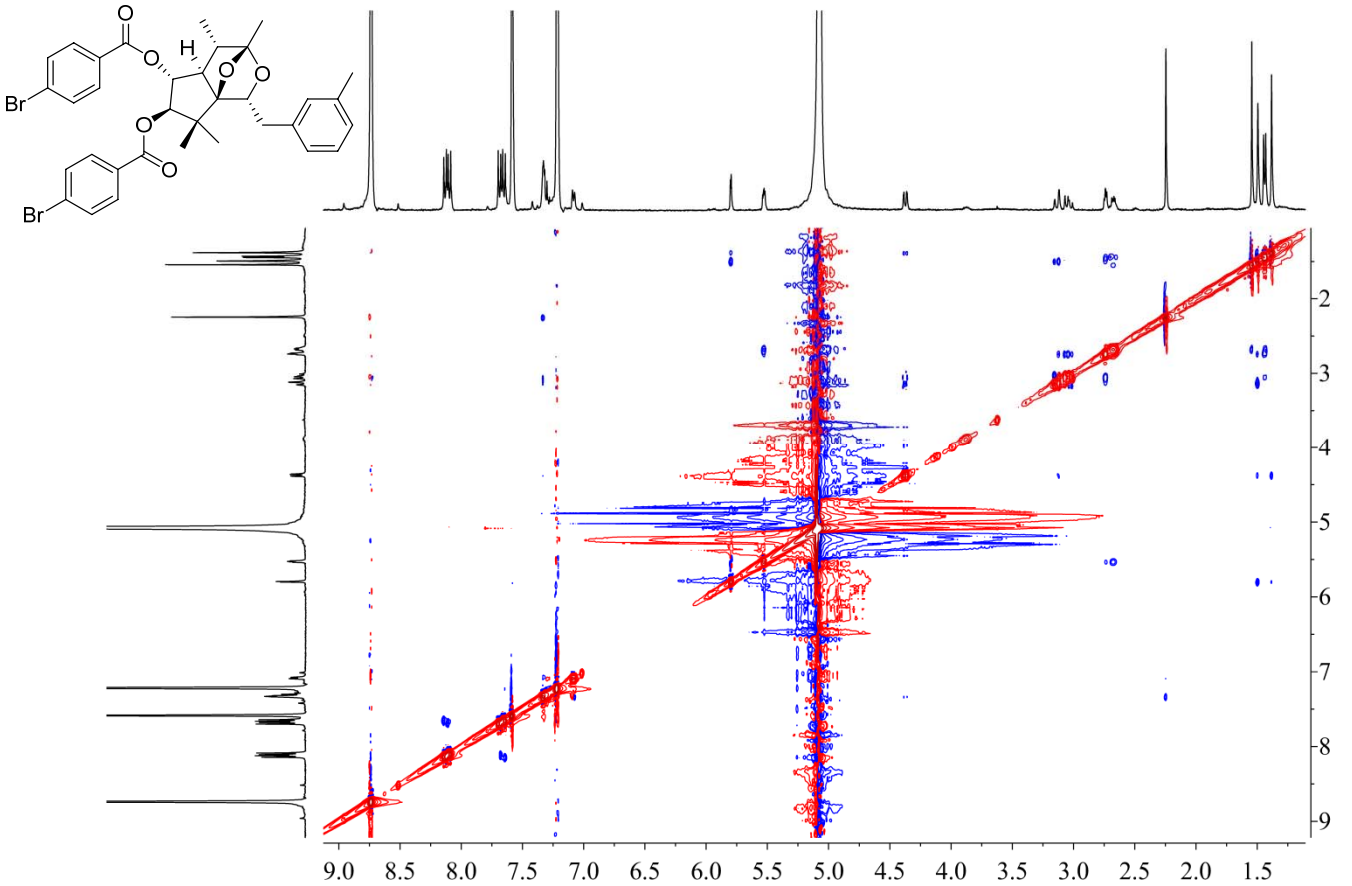

Figure S35. NOESY spectrum of **1a** (400 MHz, pyridine-d_5)

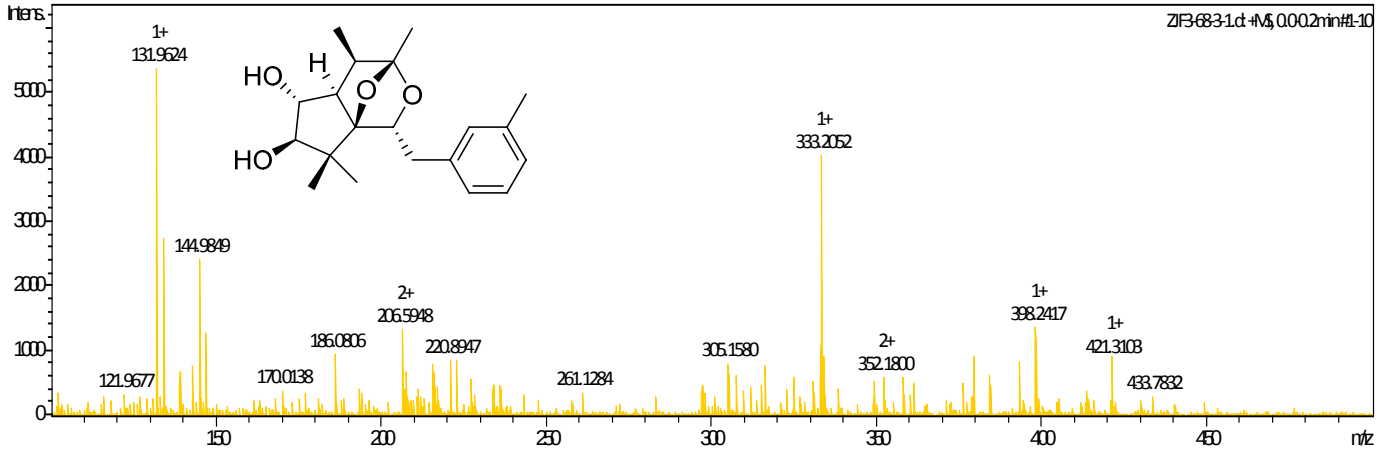

Figure S36. HR-ESI-MS spectrum of **2**

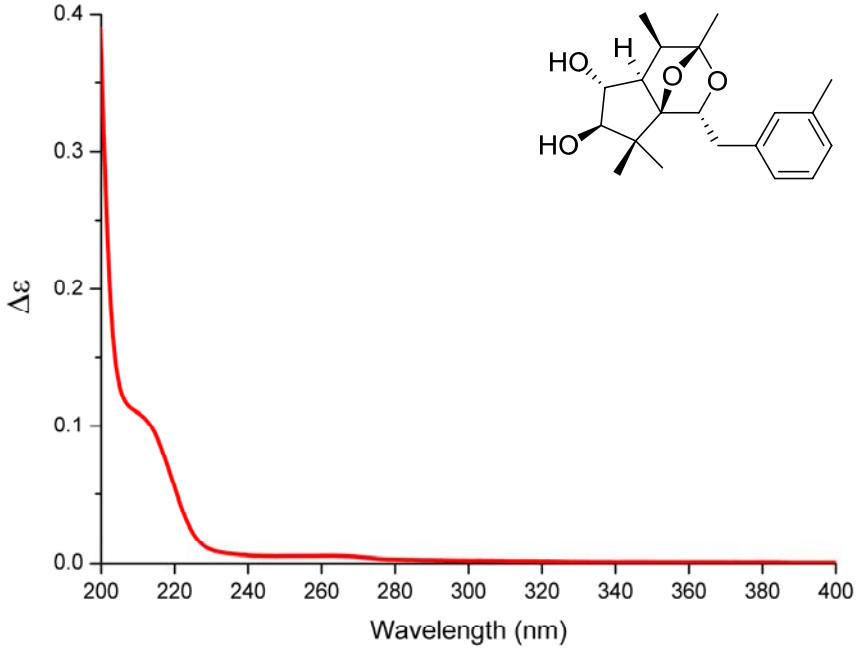

Figure S37. UV spectrum of **2** in methanol.

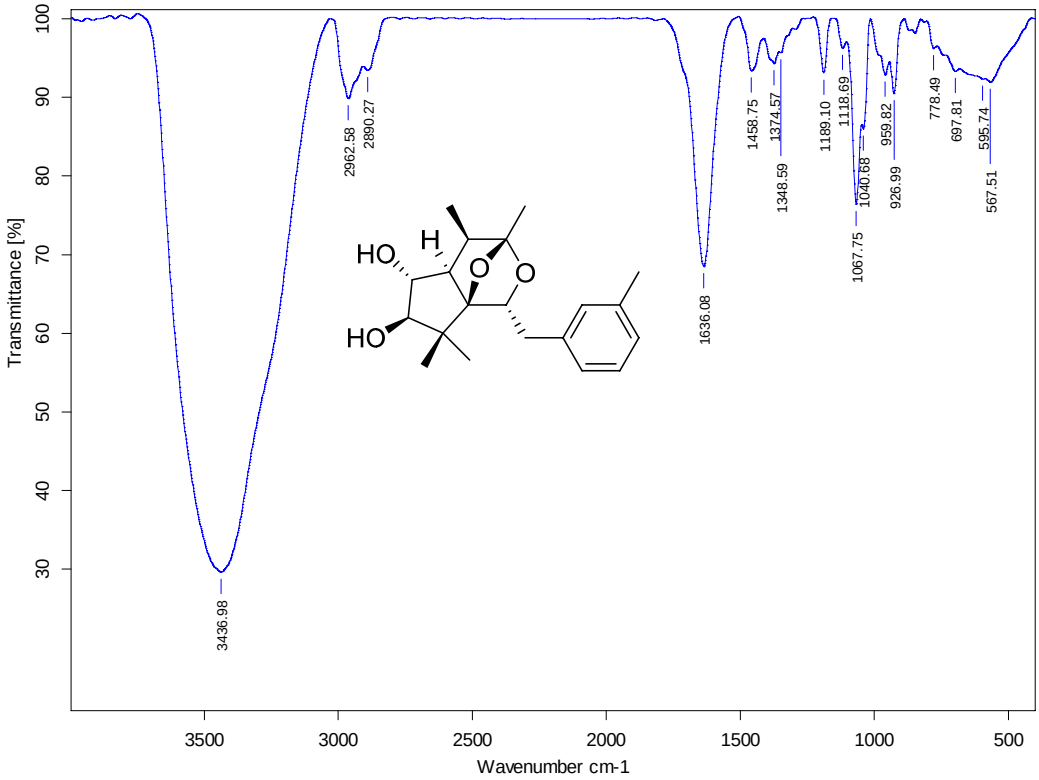

Figure S38. IR spectrum of **2** (KBr)

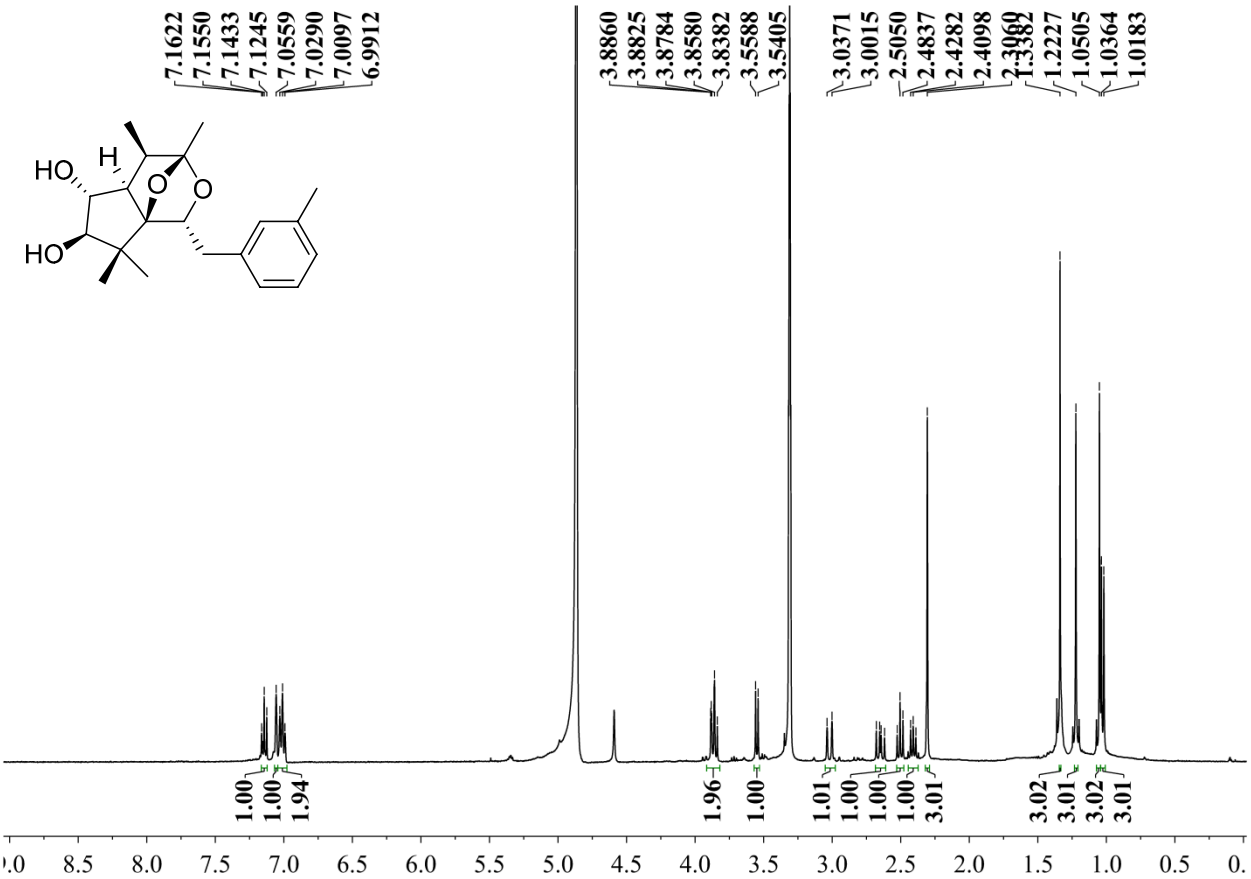

Figure S39. ^{1}H NMR spectrum of **2** (400 MHz, methanol-d_4)

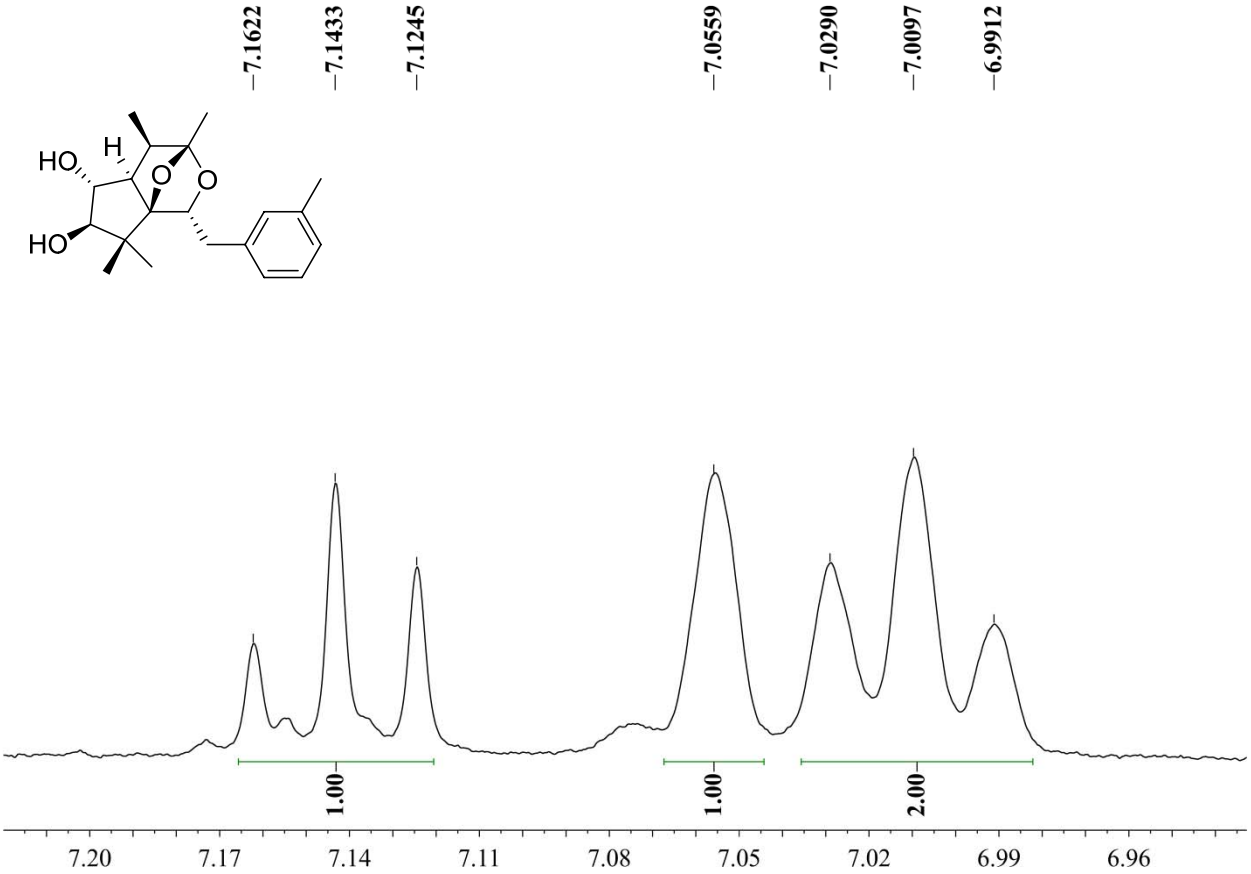

Figure S40. ^{1}H NMR spectrum (amplified) of **2** (400 MHz, methanol-d_4)

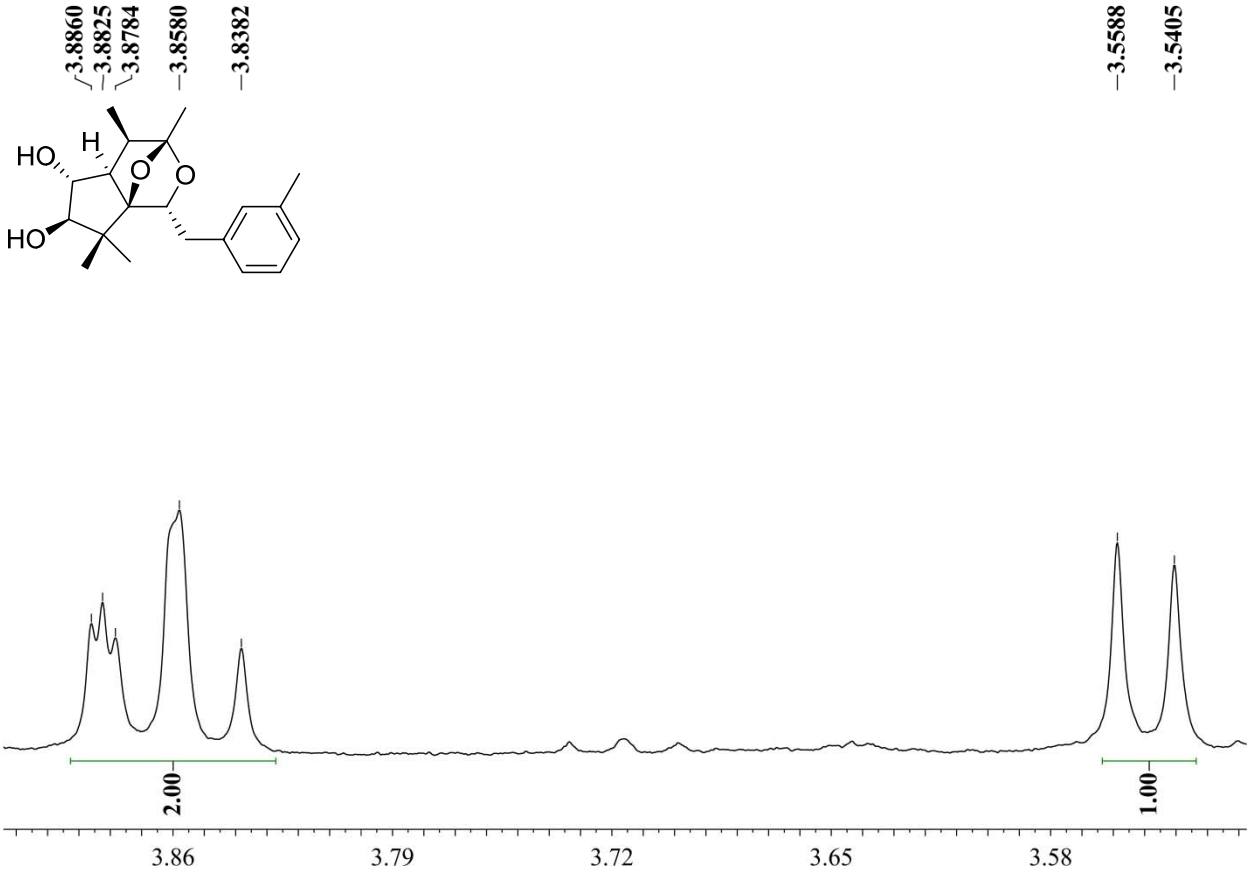

Figure S41. ^{1}H NMR spectrum (amplified) of **2** (400 MHz, methanol-d_4)

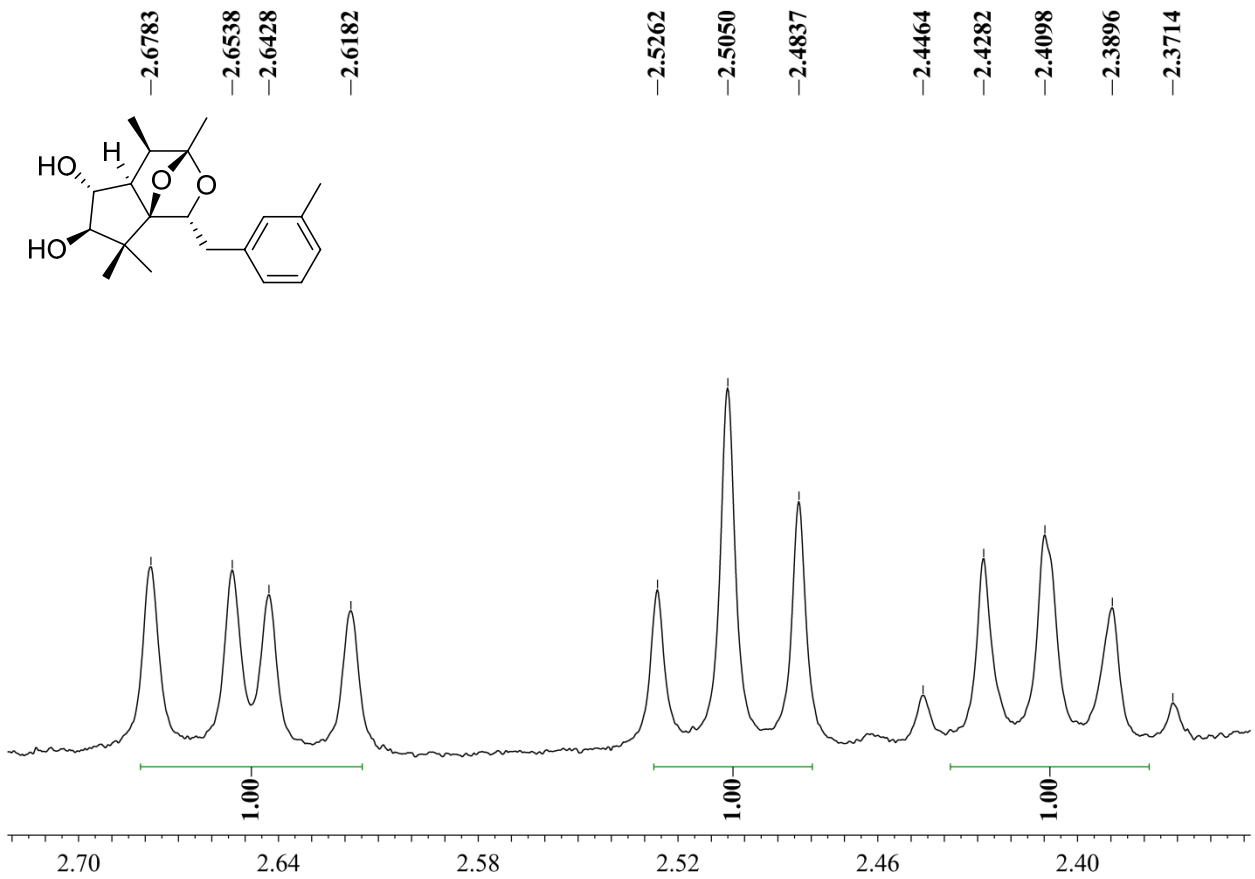

Figure S42. ^{1}H NMR spectrum (amplified) of **2** (400 MHz, methanol-d_4)

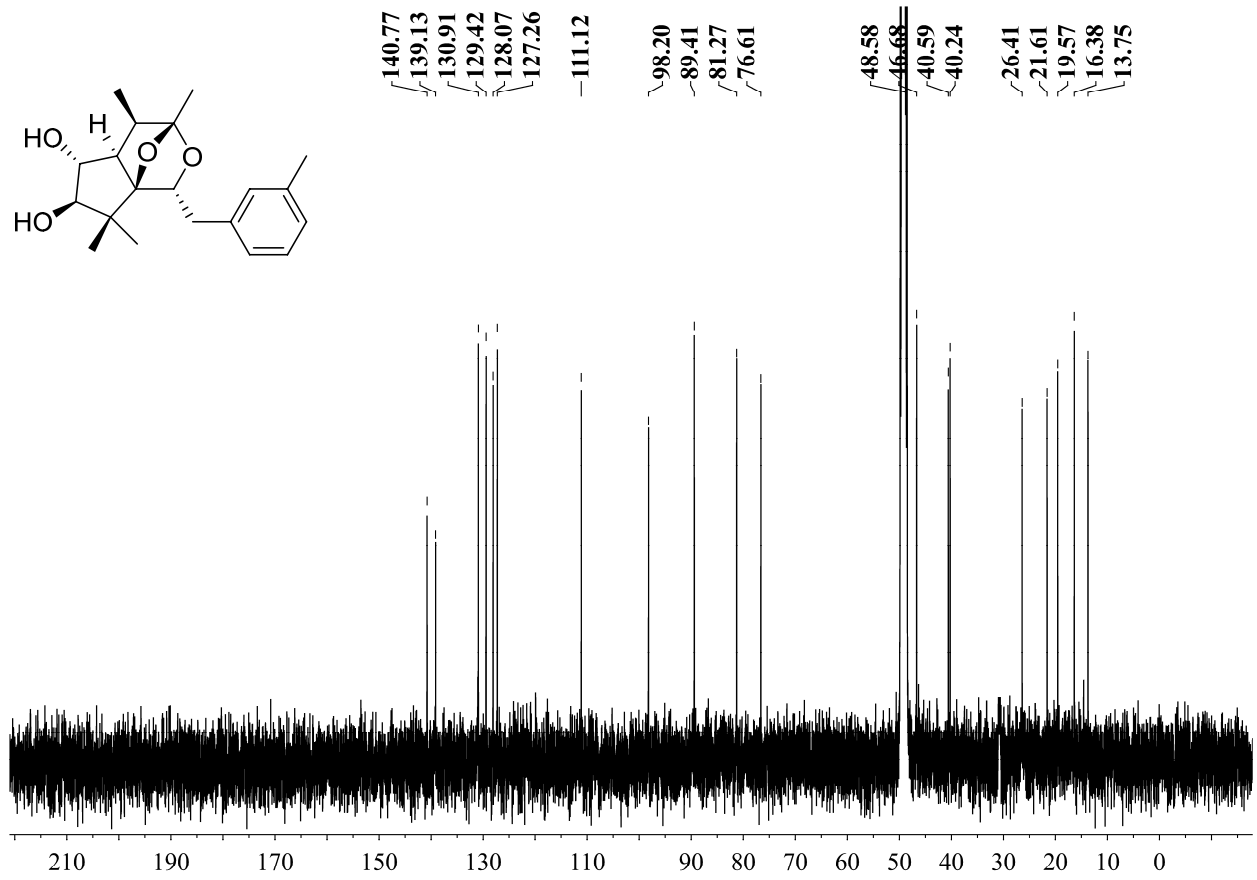

Figure S43. ^{13}C NMR spectrum of **2** (100 MHz, methanol-d_4)

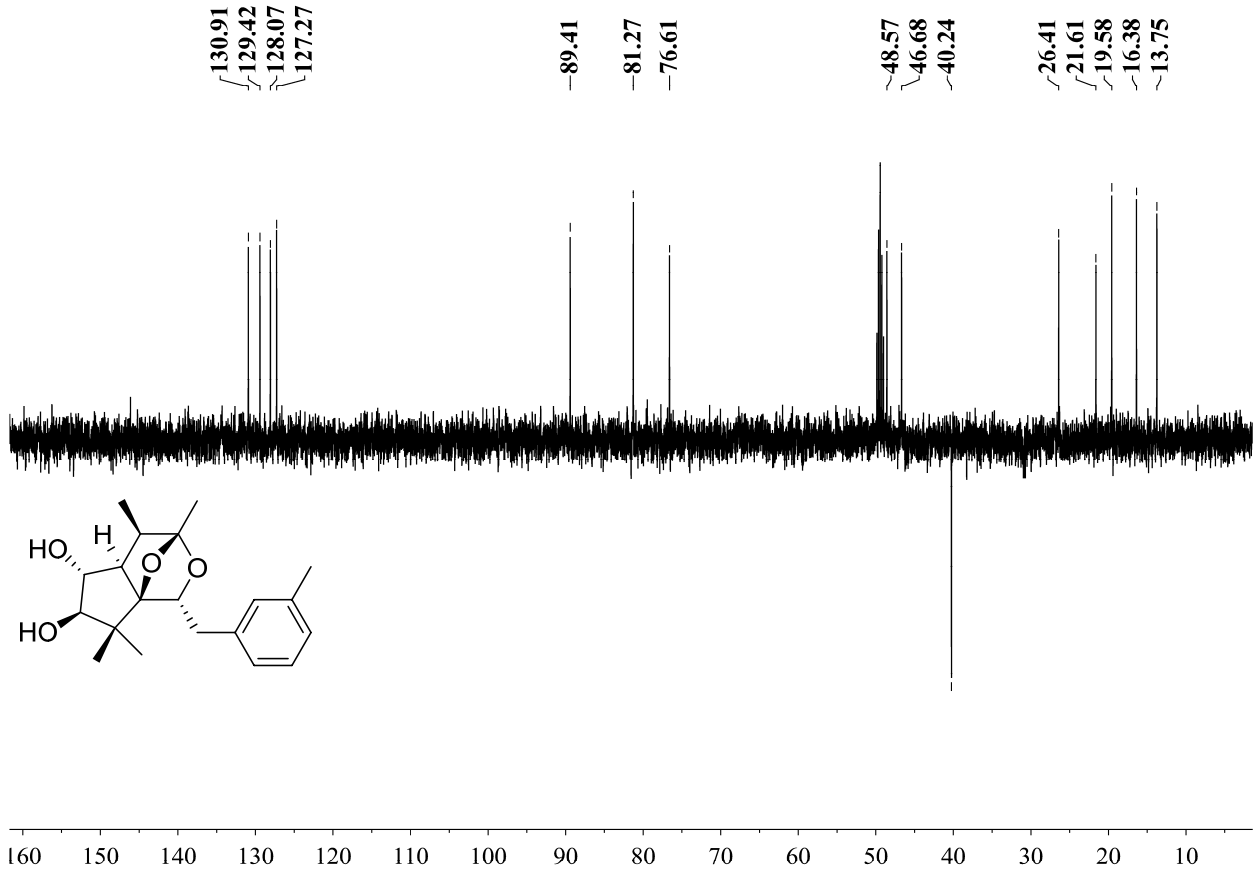

Figure S44. DEPT spectrum of **2** (100 MHz, methanol-d_4)

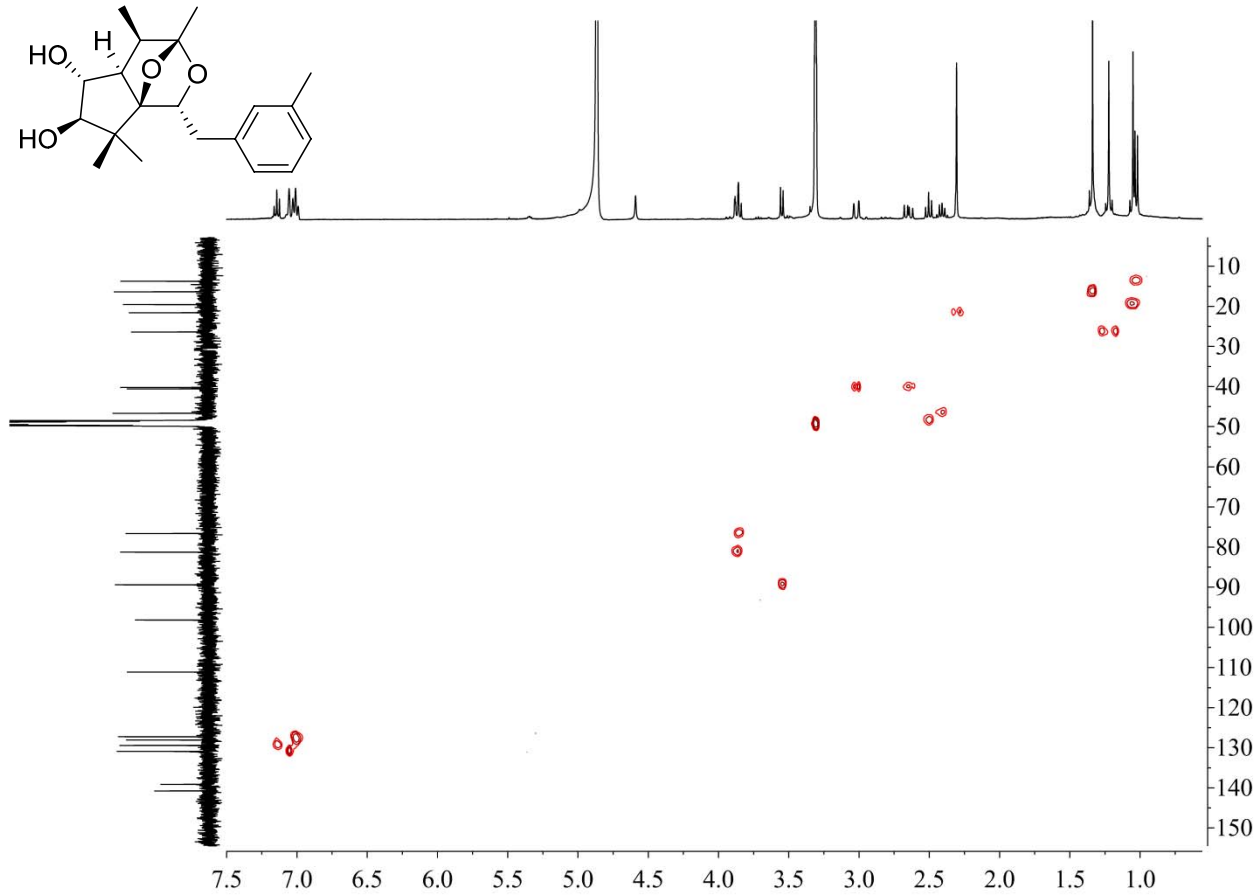

Figure S45. HSQC spectrum of **2** (^{1}H: 400 MHz, ^{13}C: 100 MHz, methanol-d_4)

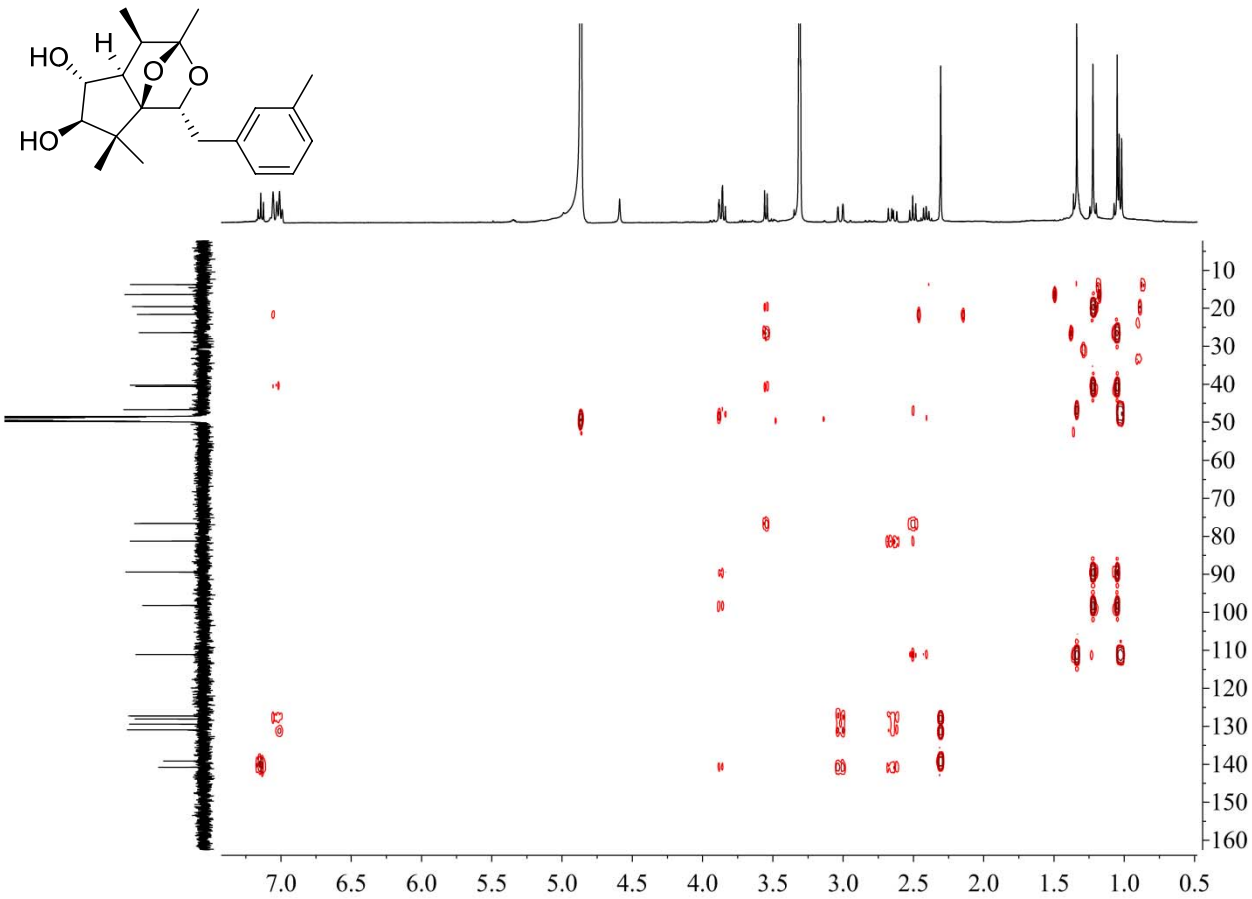

Figure S46. HMBC spectrum of **2** (^{1}H: 400 MHz, ^{13}C: 100 MHz, methanol-d_4)

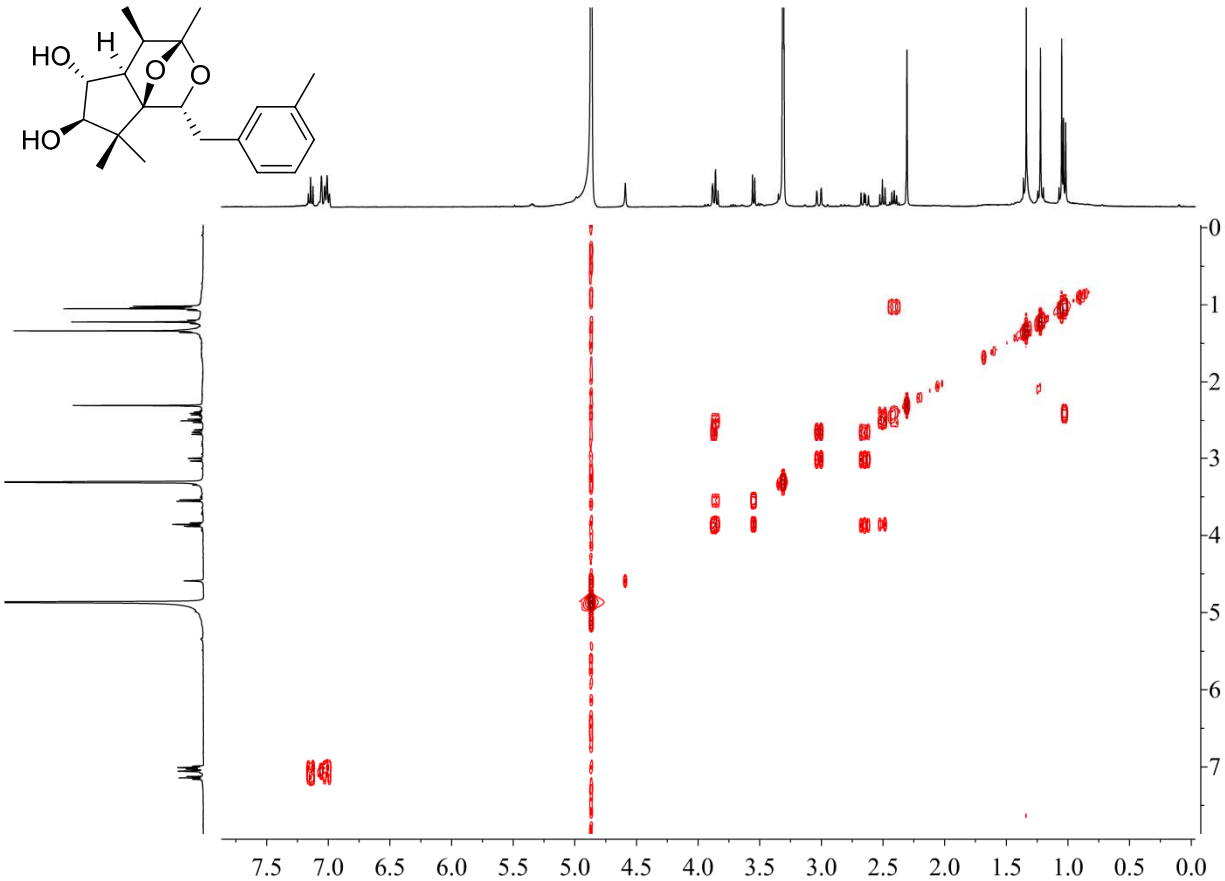

Figure S47. ^{1}H–^{1}H COSY spectrum of **2** (400 MHz, methanol-d_4)

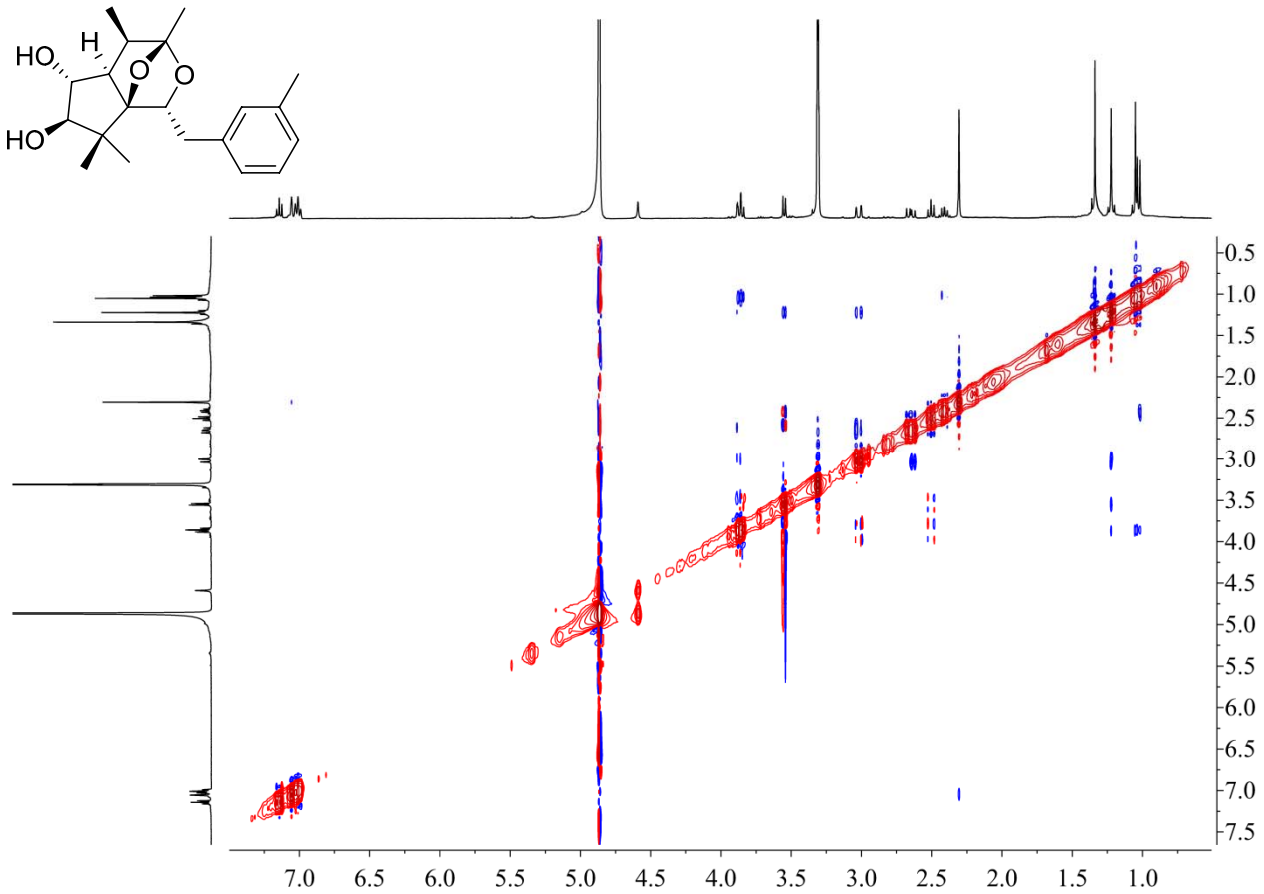

Figure S48. NOESY spectrum of **2** (400 MHz, methanol-d_4)

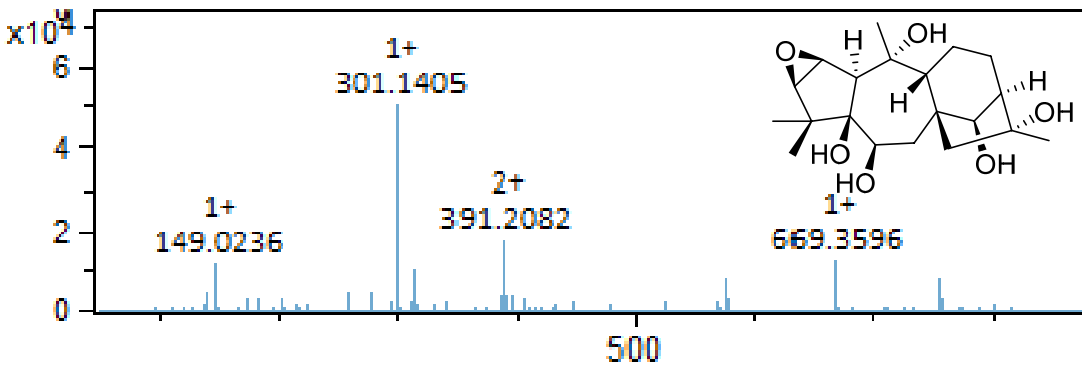

Figure S49. HR-ESI-MS spectrum of **3**

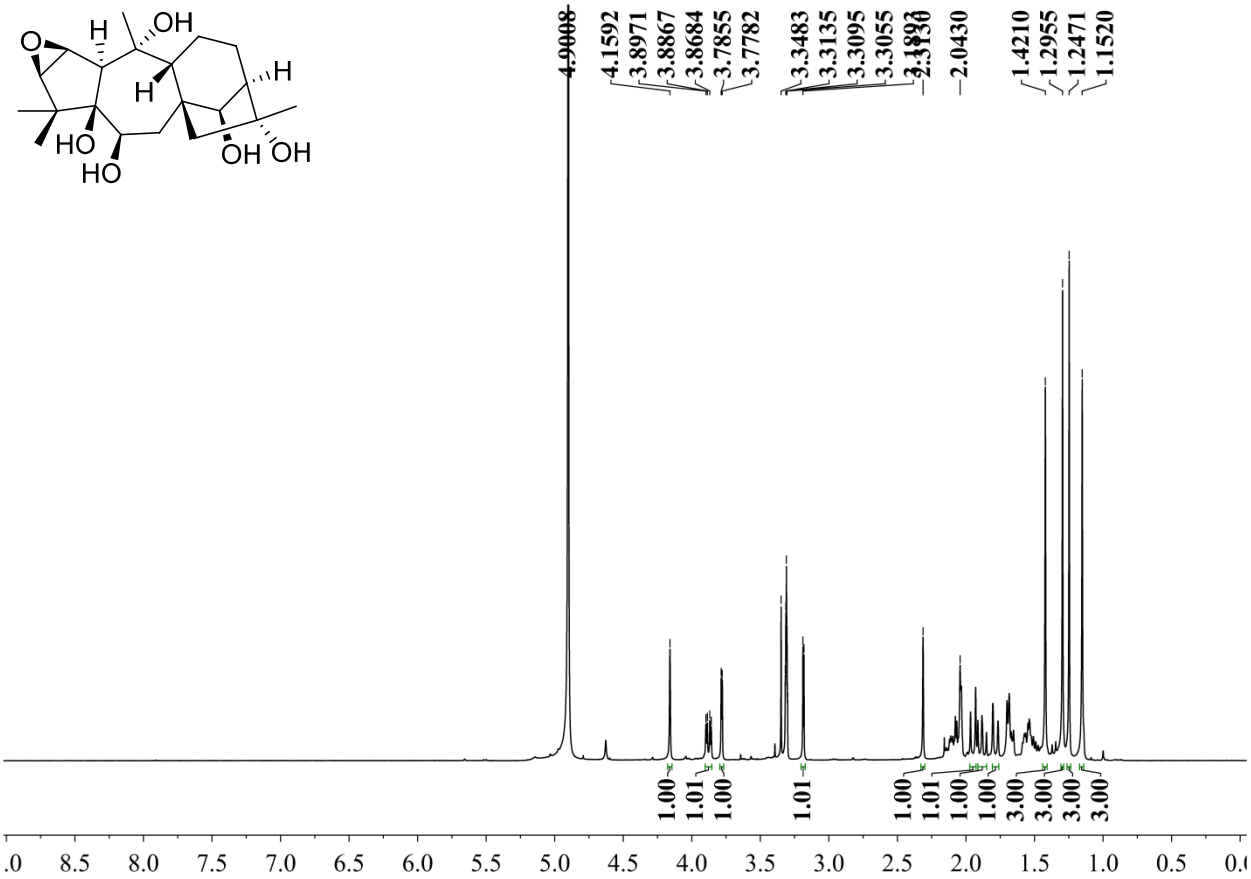

Figure S50. ^{1}H NMR spectrum of **3** (400 MHz, methanol-d_4)

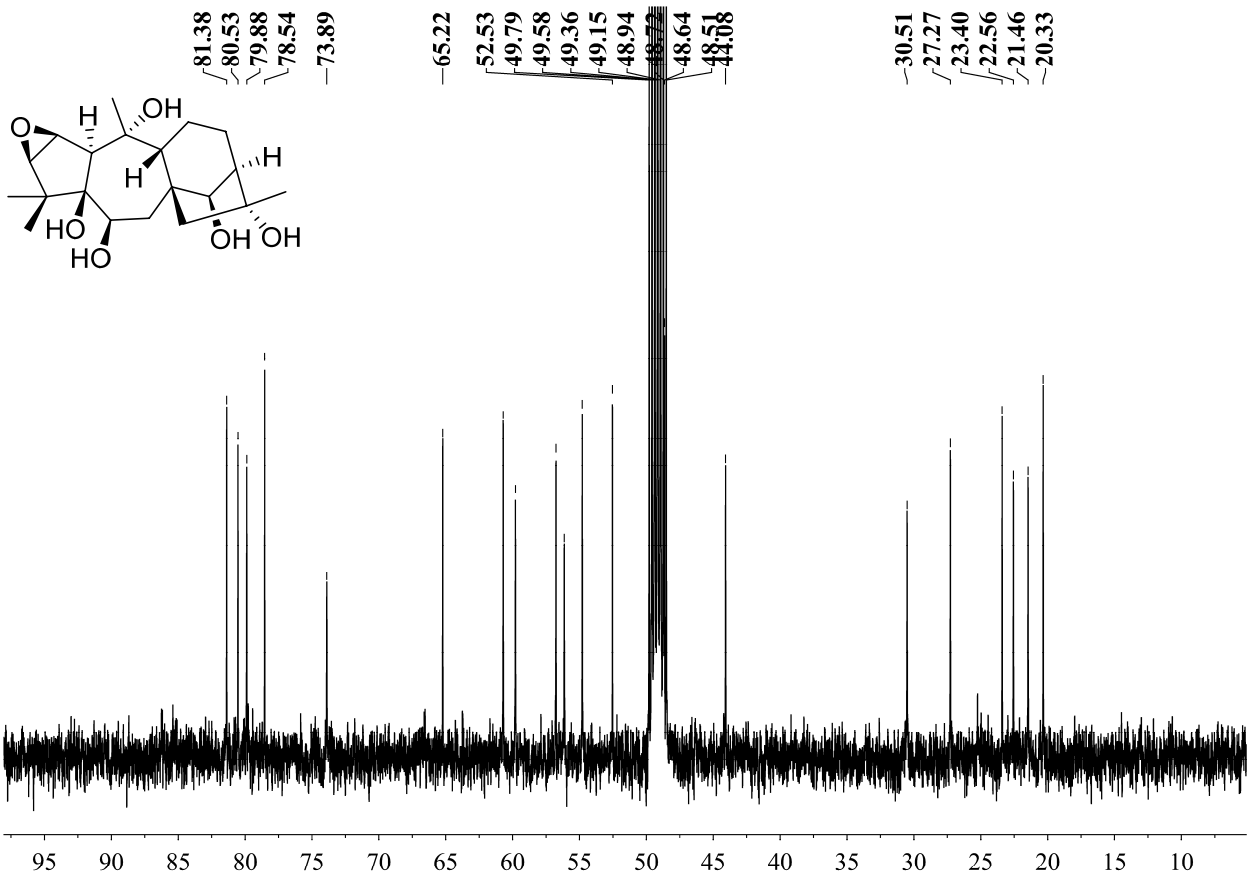

Figure S51. ^{13}C NMR spectrum of **3** (100 MHz, methanol-d_4)

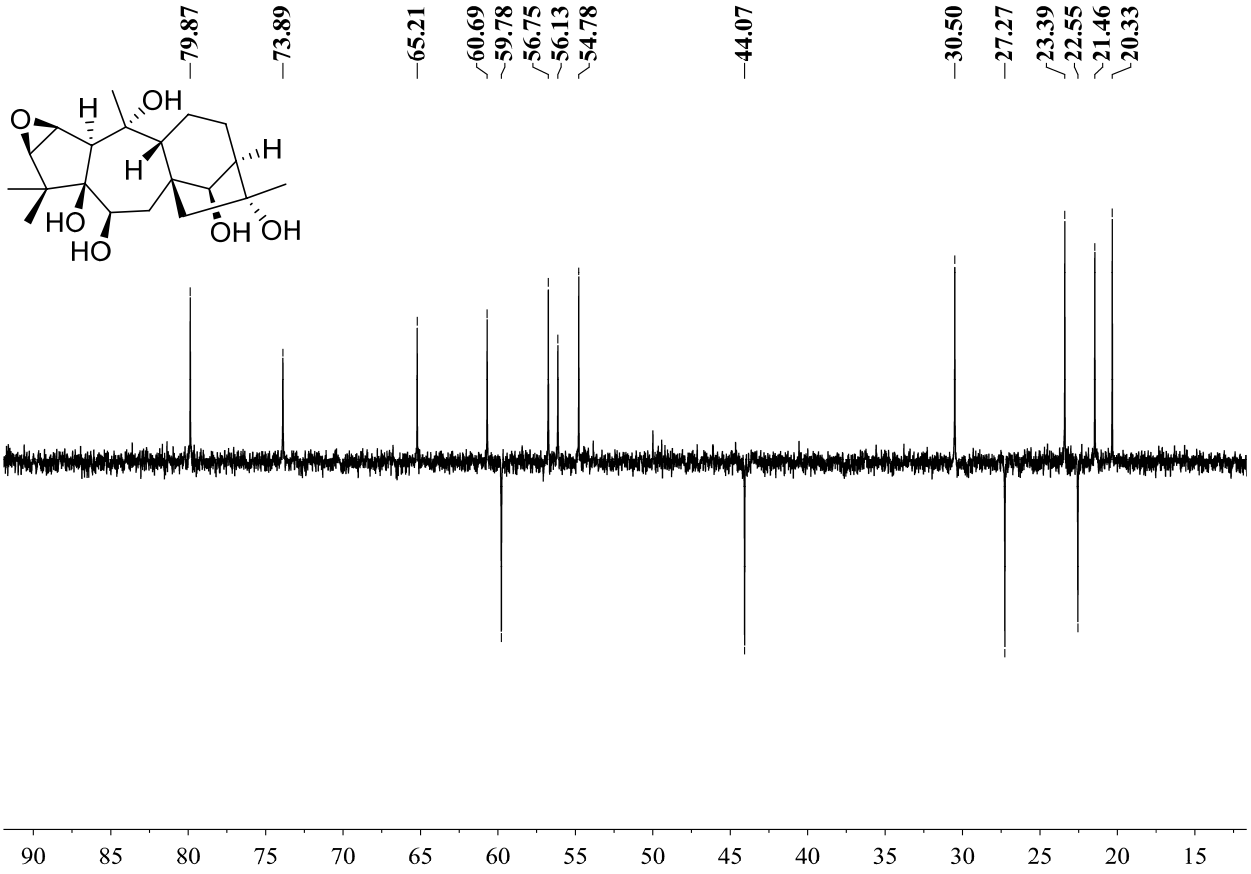

Figure S52. DEPT spectrum of **3** (100 MHz, methanol-d_4)